JGR Oceans

RESEARCH ARTICLE
10.1029/2021JC017929

Biogeochemical Timescales of Climate Change Onset and Recovery in the North Atlantic Interior Under Rapid Atmospheric CO_2 Forcing

Leonardo Bertini[1,2,3] **and Jerry Tjiputra**[4]

[1]Department of Biological Sciences, Faculty of Mathematics and Natural Sciences, University of Bergen, Bergen, Norway, [2]Marine Biology Research Group, Ghent University, Ghent, Belgium, [3]The Natural History Museum, London, UK, [4]NORCE Norwegian Research Centre, Bjerknes Centre for Climate Research, Bergen, Norway

Key Points:

- Projections reveal complex and spatially heterogeneous responses of interior biogeochemical drivers to strong CO_2 increase and mitigation
- In many parts of the North Atlantic interior, detectable anthropogenic change signals occur earlier than in the upper ocean
- In regions of relatively rapid change, interior recoveries are several centuries slower than at surface domains

Supporting Information:

Supporting Information may be found in the online version of this article.

Correspondence to:

L. Bertini and J. Tjiputra,
leonardo.bertini@imbrsea.eu;
jetj@norceresearch.no

Citation:

Bertini, L., & Tjiputra, J. (2022). Biogeochemical timescales of climate change onset and recovery in the North Atlantic interior under rapid atmospheric CO_2 forcing. *Journal of Geophysical Research: Oceans*, *127*, e2021JC017929. https://doi.org/10.1029/2021JC017929

Received 7 SEP 2021
Accepted 16 MAR 2022

Author Contributions:

Conceptualization: Leonardo Bertini, Jerry Tjiputra
Data curation: Leonardo Bertini, Jerry Tjiputra
Formal analysis: Leonardo Bertini, Jerry Tjiputra
Funding acquisition: Jerry Tjiputra
Investigation: Leonardo Bertini, Jerry Tjiputra
Methodology: Leonardo Bertini, Jerry Tjiputra
Resources: Jerry Tjiputra
Software: Leonardo Bertini, Jerry Tjiputra

Abstract Anthropogenic climate change footprints in the ocean go beyond the mixed layer depth, with considerable impacts throughout mesopelagic and deep-ocean ecosystems. Yet, little is known about the timing of these environmental changes, their spatial extent, and the associated timescales of recovery in the ocean interior when strong mitigation strategies are involved. Here, we simulate idealized rapid climate change and mitigation scenarios using the Norwegian Earth System Model to investigate timescales of climate change onset and recovery and the extent of change in the North Atlantic (NAtl) interior relative to Pre-industrial (PI) variability across a suite of environmental drivers (Temperature—Temp; pH; Dissolved Oxygen—DO; Apparent Oxygen Utilization—AOU; Export Production—EP; and Calcite saturation state—Ω_c). We show that, below the subsurface domains, responses of these drivers are asymmetric and detached from the anthropogenic forcing with large spatial variations. Vast regions of the interior NAtl experience detectable anthropogenic signals significantly earlier and over a longer period than those projected for the near-surface. In contrast to surface domains, the NAtl interior remains largely warmer relative to PI (up to +50%) following the mitigation scenario, with anomalously lower EP, pH, and Ω_c (up to −20%) south of 30°N. Oxygen overshoot in the upper mesopelagic of up to +20% is simulated, mainly driven by a decrease in consumption during remineralization. Our study highlights the need for long-term commitment focused on pelagic and deep-water ecosystem monitoring to fully understand the impact of anthropogenic climate change on the North Atlantic biogeochemistry.

Plain Language Summary Widespread climate change and increasing CO_2 emissions have effects that go beyond the ocean surface, impacting ecosystems in the deep ocean. However, the timing of changes is poorly understood, much less where particularly responsive or unresponsive areas occur following mitigation toward Pre-Industrial atmospheric CO_2. We use a numerical model to simulate the Earth system and its major physicochemical, geological, and biological processes in the atmosphere, hydrosphere, and lithosphere. We forced the model with strong and steady injection followed by strong removal of atmospheric CO_2 back to Pre-Industrial levels to understand the responses of seawater properties in the North Atlantic interior (Temperature, pH, Dissolved Oxygen). We find that southern portions of the North Atlantic interior remained up to 50% warmer and inhospitable to calcifying organisms even after returning the atmosphere to the Pre-Industrial state and allowing several centuries for the oceans to readjust. A counterintuitive accumulation of oxygen in the ocean interior is also simulated, despite reduced solubility in warmer seawater temperatures, mainly driven by reduced export and consumption of organic matter at depth. Further studies are needed to better understand the impact of anthropogenic climate change and mitigation actions to safeguard the ecosystems of the deeper parts of our oceans.

1. Introduction

Ocean biogeochemistry is expected to change because of future climate change, with apparent consequences for marine ecosystem services that are essential for human well-being (IPCC, 2019). These changes are a result of direct and indirect impacts on the climate system and involve not only warming due to increasing greenhouse gases but also subsequent changes in the large-scale circulation of the global ocean. Many studies investigating future climate change projections have highlighted that it is not just the surface and subsurface layers of the oceans which are subject to significant change because of anthropogenic forcing. The ocean interior is also

Supervision: Jerry Tjiputra
Validation: Jerry Tjiputra
Visualization: Leonardo Bertini, Jerry Tjiputra
Writing – original draft: Leonardo Bertini
Writing – review & editing: Leonardo Bertini, Jerry Tjiputra

affected by either direct or indirect effects of global warming as the oceans become more stratified and the main gateways for deep ocean ventilation and rates of heat and carbon sinks are compromised (Caesar et al., 2020; Gehlen et al., 2014; Sarmiento & Le Quere, 1996).

The North Atlantic (NAtl) is one of the regions of great interest to study the long-term effects of climate change given its close coupling with the atmosphere. Responses of ocean biogeochemistry to climate change are expected to be particularly stronger in zones of deep convection of the NAtl with cascading effects throughout the ocean interior via changes in the Atlantic Meridional Overturning Circulation (AMOC). The thermohaline circulation in the NAtl is largely responsible for triggering the global overturning circulation and the deep ventilation via the formation of North Atlantic Deep Water (NADW), constituting the major gateway through which anthropogenic CO_2 penetrates the interior and deep ocean on a global scale (Tjiputra, Assmann, & Heinze, 2010; Völker et al., 2002). This close coupling with the atmosphere is not only strongly linked to interannual to multi-decadal climate variability (Chen & Tung, 2018) but also very sensitive to long-term climate change (Goris et al., 2015; Zickfeld et al., 2008).

Global warming increases ocean stratification and weakens the AMOC, leading to a reduction in the rate of transfer of anthropogenic heat and carbon from the surface to the ocean interior (Gehlen et al., 2014; Katavouta & Williams, 2021; Sarmiento & Le Quere, 1996), but also to a redistribution of the Pre-industrial (PI) ocean heat and carbon content (Caesar et al., 2020; Winton et al., 2013). At the same time, a weakened AMOC increases the accumulation and storage of remineralized carbon at depth on centennial timescales despite decreasing export production (Bernardello et al., 2014; Katavouta & Williams, 2021). Observational research suggests that the strength of the AMOC has decreased at an annual rate of 7% between 2004 and 2012 (Smeed et al., 2014). This is mainly attributed to the melting of ice caps which leads to the freshening of seawater in subduction zones. The loss of sea-ice reduces albedo, further contributing to the increase in sea surface temperature (SST), forming a positive feedback mechanism (Box et al., 2012). As a result, water column stability increases in high latitudes, which translates not only into the weakening of the AMOC but also in changes in biogeochemical properties as stratification hinders nutrient supply and affects the turnover of organic matter throughout the water column.

Changes in thermohaline circulation and ocean biogeochemistry could lead to decreases in ocean productivity and can ultimately disrupt marine ecosystem services that are critical to human livelihood, with impacts already evident at higher latitudes (Wassmann et al., 2011). The long-term consequences of these shifts for the global ocean carbon cycle and, in particular, the biological pump are still largely unknown. And so are the possible effects on the restructuring of biological communities in the ocean interior, which depend largely on the export of particulate organic carbon (Export Production, EP) that is produced within the mixed layer (Jones et al., 2014; Ramirez-Llodra et al., 2011; Whitt & Jansen, 2020).

Habitats of the NAtl interior (i.e., the mesopelagic and deep ocean) are amongst the ones which will face the greatest challenges (Levin & Le Bris, 2015). Not only do these regions depend largely on the organic matter sinking from well-lit layers, but all benthic and demersal life forms in these environments have also evolved in relatively stable conditions and withstand only small fluctuations in physical and biogeochemical properties, such as Temperature (Temp), Dissolved Oxygen (DO), Export Production (EP), and Calcite Saturation State (Ω_c). For instance, the mesopelagic NAtl is home to vast communities of cold water corals (CWC), some of which are thousands of years old and stretch out for more than 30 km (Buhl-Mortensen et al., 2015; Costello et al., 2005). These reefs support a diverse community of commercially important fish and associated detritivores (Baillon et al., 2012; Henry et al., 2013). Furthermore, the mesopelagic ocean is also home to the largest fish communities on Earth. Irigoien et al. (2014) suggest that the biomass of mesopelagic fish could be 100 times greater than the global marine fisheries (~100 million tons - (FAO, 2018)).

Previous studies have focused on understanding how biogeochemical properties in the surface ocean are changing in the face of global warming and ocean acidification (Courtney et al., 2017; Kwiatkowski et al., 2020; Meyer & Riebesell, 2015; Riebesell et al., 2018; Webster et al., 2016) presumably because the epipelagic is the domain closest to human interactions and deep ocean species are less likely to be the first affected by changes in SST (Coll et al., 2020). However, given the importance of NAtl interior in regulating climate change and supporting life, an assessment of climate change impacts on this domain is of great relevance (Hidalgo & Browman, 2019). Presently, only a few studies have addressed the possible effects of climate change on the biogeochemistry and biology of the mesopelagic regions of the world's ocean (Brito-Morales et al., 2020; Guinotte et al., 2006; Hebbeln

et al., 2019; Hennige et al., 2015; Puerta et al., 2020) and little is known about the implications of climate change recovery following the implementation of strong mitigation strategies (Cao et al., 2014; John et al., 2015). The timescales of climate change emergence and recovery under such scenarios are poorly understood and so are the mechanisms constraining the associated spatial variations in the interior NAtl (Boucher et al., 2012).

It is important to consider that measures limiting future anthropogenic warming between 1.5 and 2°C above PI levels are unlikely to be realized considering current carbon emissions and the short time span for adjustment with respect to carbon-free societal and economical transformations (Friedlingstein et al., 2014; Hofmann et al., 2019; Smith et al., 2016; Steffen et al., 2018). Under this perspective, addressing ecosystem recovery using mitigation scenarios in Earth System Models is necessary since the most representative scenarios toward achieving the current Paris Agreement target would involve negative emissions (Gasser et al., 2015; Tokarska & Zickfeld, 2015). Therefore, assessing the extent to which the biogeochemistry of the NAtl interior will shift and whether mesopelagic ecosystems would be able to recover under such mitigation is fundamental if we are to aim for a manageable future in the framework of a Blue Economy. This will allow us to better understand the extent of interior ocean change and the subsequent effects of such a transition on marine ecosystem drivers.

Here we analyze the biogeochemical responses from an idealized climate change scenario of rapid warming followed by rapid cooling in the NAtl interior simulated by an IPCC-class Earth System Model (NorESM1-ME, part of the Coupled Model Intercomparison Project exercise - CMIP5). Our main objective is to evaluate the spatio-temporal evolution of key ecosystem drivers: Temp, pH, DO, EP and Ω_c throughout the different phases of the simulation.

We also investigate the reversibility of these drivers following a strong mitigation scenario and allowing for the system to readjust after returning atmospheric CO_2 (CO_{2atm}) to PI levels. More specifically, we determine: (a) the timescales associated with the onset of anthropogenic signal, (b) the extent of change throughout the different simulation phases, and (c) the persistence as well as the reversibility of the anthropogenic signal after applying mitigation, focusing on the large-scale dynamics of the North Atlantic, such as that associated with the meridional overturning circulation and large-scale biogeochemical feedbacks.

2. Material and Methods

2.1. Model System: A Short Overview

We employ the Norwegian Earth System Model (NorESM1-ME; Tjiputra et al. [2013]), which consists of atmospheric, ocean, sea-ice, and land modules. The horizontal resolution of atmospheric and continental domains is ∼2° whilst that of oceanic and sea ice is ∼1°. Oceanic fields are given in an isopycnic grid with 53 density levels and can be converted to z-coordinates of 70 regular depth levels in post-processing (Table S1). The atmospheric component is derived from the Oslo version of the NCAR Community Atmosphere Model (CAM4-Oslo; Kirkevåg et al. [2012]). The physical oceanic component is a modified version of the Miami Isopycnic Coordinate Ocean Model (MICOM; Bentsen et al. [2013]). The biogeochemical ocean module is originated from the Hamburg Oceanic Carbon Cycle model (HAMOCC; [Maier-Reimer et al., [2005]), and adapted to an isopycnic framework (Assmann et al., 2010; Tjiputra, Assmann, Bentsen, et al., 2010; Tjiputra et al., 2013). A full description and evaluation of the NorESM1-ME are available in the studies by Bentsen et al. (2013) and Tjiputra et al. (2013). A brief description of relevant representations of biogeochemical process in the model are provided in the Supporting Information (hereafter 'SI') Section 1, 'NorESM: Biogeochemical Overview'.

Most of the validations with respect to large-scale NorESM1-ME circulation features have been investigated by Bentsen et al. (2013). In that study, a first-order assessment of the model stability, the mean model state, and the internal variability of NorESM1-ME were presented. In short, when the model's mean ocean state is compared to observational data, an overall small SST bias of −0.15 K is observed with localized biases toward warming north of 60°N. In terms of sea ice extent, there is an underestimation during boreal spring and an overestimation during boreal summer in sea ice extension and thickness. The modeled AMOC strength at 26.5°N (27∼Sv) lies on the upper range of reported values for CMIP5 models (Cheng et al., 2013) and is thought to be well above estimates derived from observations between the years 2004–2011 of 17.4 Sv (Srokosz et al., 2012). Furthermore, the counter clockwise vertical abyssal circulation of Antarctic Bottom Water (AABW) is relatively weak. The relatively high AMOC intensity is also thought to induce the warm and saline biases observed mainly at depth throughout the Atlantic basin, which result from warm and saline surface water masses being even more efficiently injected

at depth and thereafter propagating southwards. Additionally, the model mean state for the Mediterranean Overflow is slightly overestimated in terms of volume transport, entering the North Atlantic interior deeper than indicated by observations. Therefore, the Mediterranean Overflow is also thought to contribute to the temperature and salinity biases observed in the interior North Atlantic, especially at ∼30°N and 3,000 m depth.

2.2. Experiment Design

Prior to any external forcing, NorESM1-ME was spun up under a PI condition (constant 284.7 ppm CO_{2atm}) for 900 years, allowing for a quasi-equilibrium state with a weak climate drift. Initial conditions for oxygen and nutrient fields were derived from the World Ocean Atlas (WOA; Garcia et al. [2010]), whereas dissolved inorganic carbon and total alkalinity values were obtained from the Global Data Analysis Project (GLODAP) data set (Key et al., 2004). The remaining biogeochemical variables in the water column are either set to zero or small but non-zero values. Further information on the spin-up phase of NorESM can be found in Tjiputra et al. (2013). After the spin-up phase, two simulations were performed: (a) a PI control (CTRL) and (b) an anthropogenic climate change simulation.

The CTRL simulation encompasses 250 model years at a PI state. The anthropogenic simulation consists of three subsequent transient phases: Ramp-up, Ramp-down, and Extension. During the Ramp-up phase, CO_{2atm} is increased at a rate of 1% yr^{-1} from the PI CO_{2atm} level for 140 years, reaching approximately four times the PI mean value. The Ramp-down illustrates an idealized scenario of rapid negative emissions where CO_{2atm} is reduced at a mirroring rate of -1% yr^{-1} for another 140 years, returning to the PI baseline. This annual rate of decrease follows the standard protocol of the Carbon Dioxide Removal Model Intercomparison Project (CDRMIP; Keller et al. [2018]). The Extension phase involves extending the anthropogenic simulation for 200 years from the end of Ramp-down (Figure 1a), where CO_{2atm} is kept at the PI value to determine the long-term responses.

Although these changes in CO_{2atm} may seem very rapid and unrealistic when compared to the observed rate (Keeling et al., 2005), they are employed to induce strong anthropogenic forcing so that anthropogenic climate change signals, both in terms of departures and recoveries, can manifest as early as possible (e.g., Schwinger & Tjiputra [2018]). Therefore, the results from this idealized scenario constitute an important tool for assessing not only the upper limits of climate change onset and climate change recovery but also the inertial responses involved in the biogeochemistry of the interior ocean over different phases of transitional forcing.

2.3. Post-Processing

Here, we use actual model outputs (i.e., not bias-corrected against observations) in our analyses and assume that changes associated with the anthropogenic forcing are more dominant than the present-day bias. We interpolate NorESM1-ME outputs from its native isopycnal vertical coordinate to regular vertical level fields when necessary (see SI for information on the interpolation and Table S1 for a list of output variables used in the study). Since the objective of this study is to understand the onset timescales and the extent of recovery in response to anthropogenic forcing, the monthly-to-seasonal variability is not of interest. We have therefore converted all monthly biogeochemical fields into annual fields. Apparent Oxygen Utilization (AOU) was determined by subtracting DO outputs from the estimated saturation concentration (O_{2sat}). O_{2sat} was determined using Temperature and Salinity fields and based on solubility coefficients from Garcia and Gordon (1992) and McDougall and Barker (2011) (see Section 2 of SI).

2.4. Timescale Analyses

Prior to conducting any timescale analyses, timeseries for all variables were corrected for model drift by subtracting the trends in the CTRL run from the anthropogenic runs. The time-related variables presented in this study were estimated for each grid box in the model. For each grid box, a range of natural variability in time was defined as two times the standard deviation of the last 30-year period of the CTRL run (2*PIsd30). This envelope (±2*PIsd30) represents the natural variability range of the respective variables (Temp, DO, etc.), meaning that any sustained deviation outside this envelope during the climate change simulation originates from external anthropogenic forcing.

Our predefined natural envelope had at its center the mean from the last 5 years of the Pre-industrial field in question (PImean5) and its upper and lower limits are given by PImean5 ± 2*PIsd30. To test how sensitive the times-

cales were to the adopted envelope, we have also computed timescales based on different envelope widths, that is, PImean5 ± 1*PIsd30 and PImean5 ± 3*PIsd30. The envelope based on a fluctuation of ±1*PIsd30 represents a more restricted condition, where departures occur earlier and recoveries later. Oppositely, the envelope based on a fluctuation of ±3*PIsd30 represents a more tolerant condition, where departures occur later and recoveries earlier (see examples in Figure S1).

We discuss our results focusing on basin-scale evolution patterns to understand the major effects of anthropogenic forcing on the NAtl. Then, we narrow down our analyses to different ocean interior zones (>200 m), which can be divided into mesopelagic (200–1,000 m) and deep ocean (>1,000 m). The deep ocean is subdivided into bathy- and abyssopelagic zones (1,000–3,000 m and >3,000 m, respectively). We present our timescale analyses along the vertical meridional section of the western Atlantic, which includes the major overturning cells both at the surface and at depth, to simplify our interpretations.

2.4.1. Time of Departure (ToD)

ToD is a concept similar to ToE (Time of Emergence; Henson et al. [2017]; Keller et al. [2014]; Tjiputra et al. [2018]). We used the terminology 'Time of Departure' because our analyses are based on a perspective where transient variability leaves predefined envelopes of natural variability. ToD is defined in our study as the point in time when there are at least 10 consecutive and non-returning model years outside the predefined envelope. ToD indicates the onset of the detectable anthropogenic signal when a particular grid point is exposed to conditions outside its PI natural variability.

2.4.2. tmax and $Tracer_{tmax}$

The point in time when the series reaches its maximum absolute change after the start of the Mitigation phase (i.e., Ramp-down) is given by t_{max}. This can be understood as the turnaround point marking the onset of the mitigation phase (i.e., from model year 140, which is when the CO_{2atm} begins to decline). In the case of pH and DO, it is expected that tmax represents the time of the global minima, since these variables are expected to decrease with climate change and increasing CO_{2atm}, whereas for Temperature tmax represents the time of maximum warming ($Temp_{tmax}$). The values associated with tmax are given by $Tracer_{tmax}$, which is the maximum or minimum value experienced at a grid point over the entire simulation period.

2.4.3. Trec

When the time-series re-enters the natural variability envelope within the duration of the experiment, Trec is defined as the first point in time when the series returns to the envelope and remains in it for at least 10 consecutive years. If the series does not show a sustained return of at least 10 years, linear regression is calculated using the last 100 years of the Extension phase to estimate Trec (see examples in Figure S2).

2.4.4. Time-Slices Percentage Change

To identify which regions have significantly changed over the course of the anthropogenic simulation compared to the PI, statistical analyses of percentage change of both physical and biogeochemical fields were carried out using 30-year windows (paired t-tests at a significance level $\alpha = 0.05$). The periods compared against the last 30 years of the PI were: (a) the last 30 years of the Mitigation phase (model years 250–280), (b) the middle of the Extension phase (model years 350–380), and (c) the last 30 years of the Extension phase (model years 450–480). Data flagging was conducted to mark where significant changes were observed with respect to the PI.

3. Results and Discussion

Our simulation of strong anthropogenic forcing using NorESM1-ME reveals large-scale changes that are consistent with other models as previously documented (e.g., Bopp et al. [2013]; Schwinger & Tjiputra [2018], among others). Warming, deoxygenation, ocean acidification, weakening of AMOC, increased stratification, reduced surface productivity, and reduced sea ice cover are prevalent throughout the Ramp-up phase (Figures 1 and S3-S5 in SI). During Ramp-down (i.e., mitigation phase), some of these changes revert to the PI state, while others show a lagged response at asymmetric rates and did not show signs of recovery toward PI levels.

Area-weighted and volume-weighted results for the NAtl (0–65°N) reveal that the mean SST and the water column Temperature increased by 0.13°C and 0.70°C by the end of the climate change simulation, respectively

(Figure 1b). The mean surface pH returns to the PI value while water column pH decreases by 0.025 units (Figure 1c). The mean water column DO and AOU decreased by 1.47 μmol kg^{-1} and 3.60 μmol kg^{-1}, respectively (Figure 1d). This suggests that warming and deoxygenation relative to the PI persist, even after the Extension phase. AMOC strength is inversely correlated with the increase in CO_2 forcing and warming, which is consistent with other ESM projections (Cheng et al., 2013; Weijer et al., 2020). The simulated AMOC strength shows a lagged response toward a rebound, with a minimum in strength being projected several years into the Ramp-down and plateauing over the Extension phase at approximately PI level (Figure 1e). The response of sea ice cover in the Arctic shows a sharp decrease over the Ramp-up and an immediate rebound as soon as mitigation starts, however stabilizing at lower levels than in the PI over the Extension phase (Figure 1f).

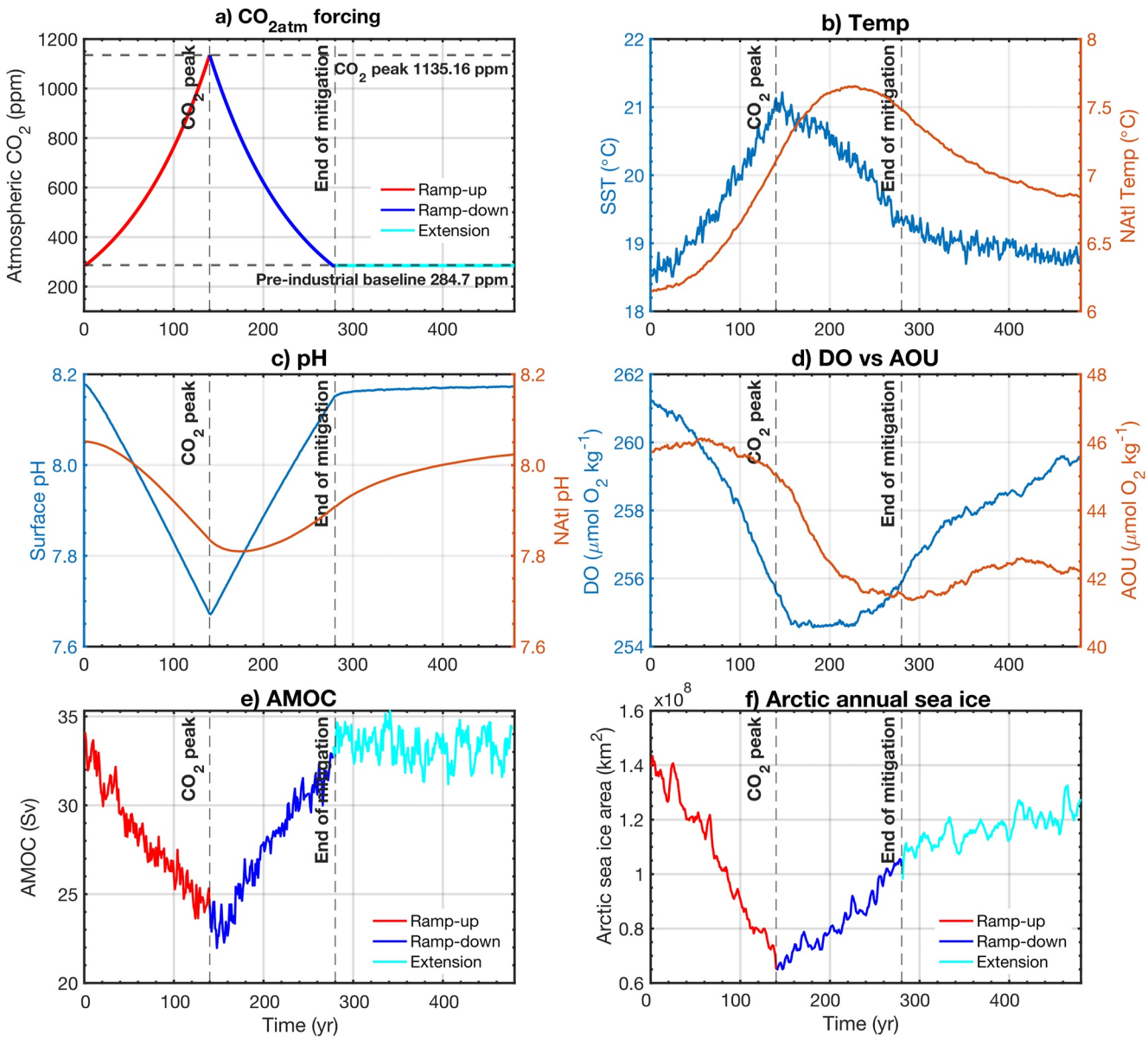

Figure 1. NorESM1-ME transient evolution of (a) prescribed atmospheric CO_2 forcing; North Atlantic (0–65°N), (b) area-weighted mean sea surface Temperature (SST) in light blue and volume-weighted mean water column Temperature (NAtl Temp) in orange, (c) area-weighted mean seawater surface pH in light blue and volume-weighted mean water column pH in orange; (d) volume-weighted water column mean Dissolved Oxygen (DO) in light blue and Apparent Oxygen Utilization (AOU) in orange; (e) maximum Atlantic Meridional Overturning Circulation strength between 20 and 60°N and (f) Evolution of Arctic sea ice area. Legends in panels (a), (e) and (f) show data for Ramp-up in bold red, Ram-down in deep blue, and Extension phase in cyan.

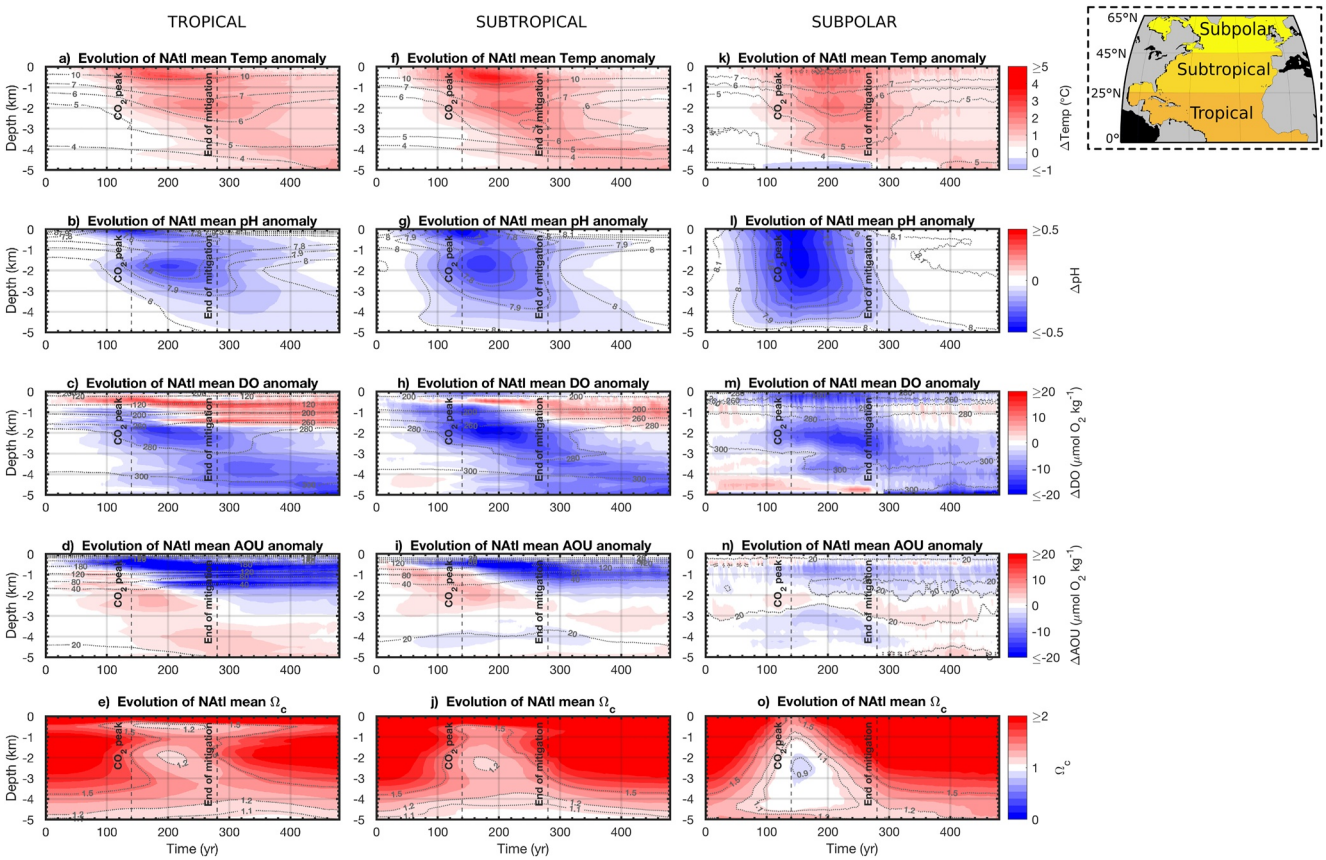

Figure 2. NorESM1-ME temporal evolution of mean vertical profiles of volume-weighted anomalies for (a,f,k) Temperature (Temp), (b,g,l) pH, (c,h,m) Dissolved Oxygen (DO), (d,i,n) Apparent Oxygen Utilization (AOU) and (e,j,o) mean vertical profiles of volume-weighted Calcite saturation state (Ω_c) throughout the simulation for the North Atlantic according to latitudinal bands (upper right corner: map in dashed box). Tropical: panels a-e, 0–25°N; Subtropical: panels f-j, 25–45°N and Subpolar: panels k-o, 45–65°N. Dashed vertical lines mark model year 140, when CO_{2atm} reaches its peak in the atmosphere (1,135.16 ppm) and model year 280, when the mitigation trend stopped and CO_{2atm} returned to the PI baseline (284.7 ppm). Isolines indicate actual values.

Next, we explore changes in Temp, pH, DO, AOU and Ω_c, as well as EP separately, focusing our temporal analysis on (a) subdividing the NAtl into latitudinal domains (tropical, subtropical, and subpolar) and (b) a depth section along a meridional transect on the Western NAtl (i.e., encompassing the major overturning cells both at the surface and at depth) to better distinguish between different spatial controls.

3.1. Temperature (Temp)

The evolution of the mean Temperature vertical profile shows that the warming signal in the interior NAtl is more pronounced in the subpolar domain (45–65°N), where isotherms start to deepen halfway through Ramp-up, whereas the warming response is slower in the subtropical (25–45°N) and tropical domains (0–25°N; Figures 2a, 2f and 2k). Our results suggest an increase in Temperature by as much as +3°C between 500 and 2,000 m depth, especially in the subpolar NAtl (see SI Animation S1 for the evolution of ΔTemp over different depth layers). At the end of the simulation, in the upper 1,000 m of the tropical and subtropical domains, the mean Temperature state tends to return to PI levels (Figures 2a and 2f). However, the propagation of the warming signal continues at depth (>3,500 m). Isotherms in the deep subpolar mesopelagic (2,000–3,000 m) are still deepened by more than 500 m from their PI position and by more than 1,000 m in the deep NAtl (>3,000 m, Figure 2k).

The vertical profile based on an envelope of 2PIsd suggests that the mean Temperature ToD is delayed in the upper NAtl (Figure 3a), with moderate values of ToD (60 ± 10 years) in the first 50 m of the water column, followed by a zone of climate change buffering down to 200 m encompassing the highly variable thermocline,

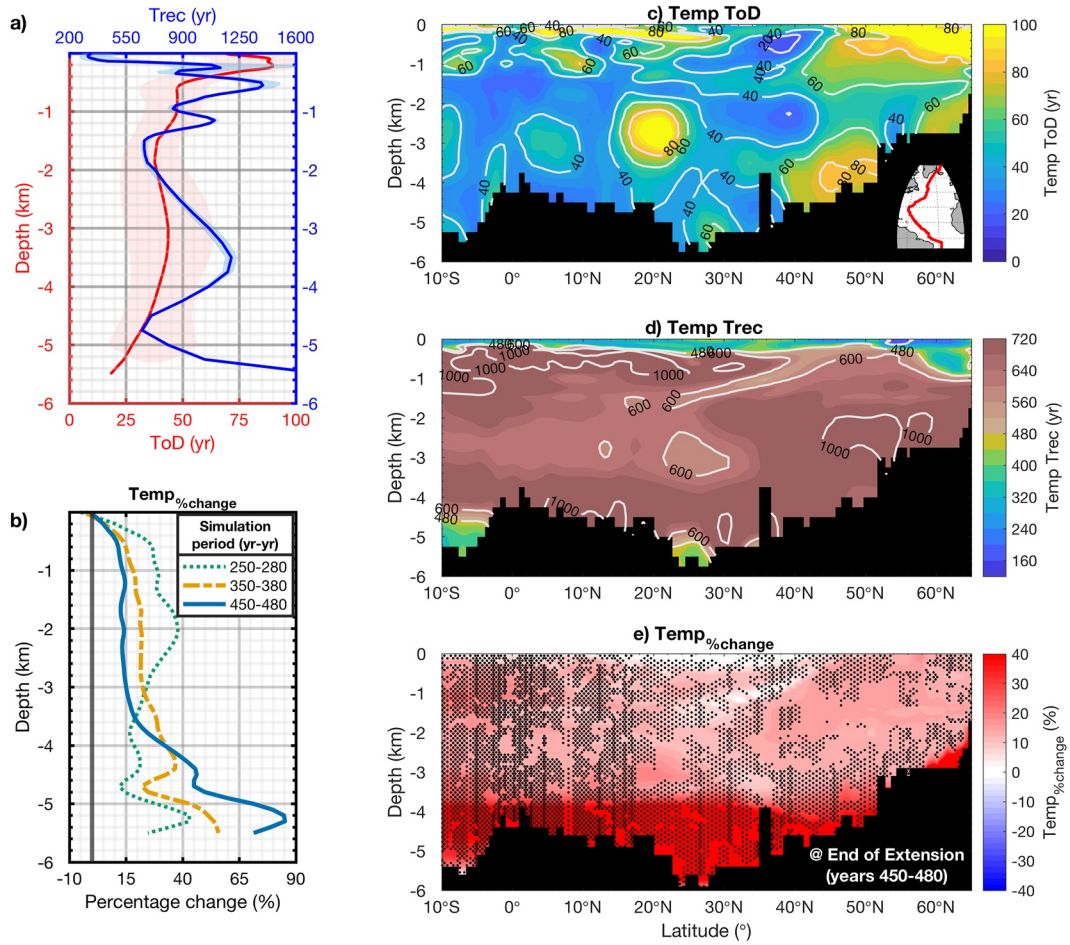

Figure 3. NorESM1-ME North Atlantic (0–65°N) volume-weighted vertical profiles of (a) mean Temperature (Temp) ToD and Trec (yr), solid red and blue lines respectively and (b) mean Temperature percentage change ($Temp_{\%change}$), across different simulation periods: years 250–280 (end of Mitigation phase), years 350–380 (halfway through the Extension phase) and years 350–380 (end of Extension phase); panels c-e show the meridional section along the western side of the basin (i.e., along the red transect in panel c, bottom right corner) of mean Temperature (c) ToD, (d) Trec, with brown-shaded areas indicating recovery outside the time span of the simulation (>480 years), and (e) percentage change (%) at the end of the Extension phase. Stippling in (e) indicates regions of significant differences relative to the PI values. Units in (a, c, d) are model years since the start of the simulation. Shading around solid lines in panel (a) represent uncertainty range estimated using different natural variability envelopes (see Section 2.4).

marked by the highest ToD (85 ± 40 years). Below the thermocline, Temperature ToD decreases throughout the mesopelagic NAtl, reaching values of 40 ± 10 years.

The meridional section along the western NAtl shows relatively later departures in the mesopelagic north of 40°N (Figure 3c). South of 40°N, ToD values decrease throughout the mesopelagic, indicating domains that are more sensitive to climate change with respect to fluctuations in Temperature. Time of recovery (Trec) estimates show virtually no recovery within the time span of the simulation, with projected values no lower than 700 years occurring throughout most parts of the NAtl section (Figure 3d). The exceptions were the very bottom (4,500–5,000 m), with Trec ranging between 300 and 450 years and the very surface (<200 m), where Trec values ranged between 320 and 400 years.

At the very surface between 45 and 50°N, a patch of low Trec values (<200 years) is simulated. This marks a region where a cooling trend has been detected (not shown). In this patch, Temperatures up to 10% cooler are projected at the end of the Extension phase, with its position varying eastwards at depth (Figures S6 and S7). This feature is also present in other models (Drijfhout et al., 2012) and is referred to as the Warming Hole. Its formation is associated with the slowdown in AMOC strength, which reduces low-latitude heat transport into

the region. Other mechanisms such as aerosol forcing and increased heat transport from the subpolar to high latitudes in other models have also been shown to affect the Warming Hole formation (Dagan et al., 2020; Keil et al., 2020).

The model projects NAtl interior to be 15% warmer basin-wide, even after mitigating emissions and allowing for 200 years of extension time (Figure 3b blue solid line). The top 3,000 m of the water column warmed up by +40% after the Mitigation phase, gradually decreasing to +25% and then +15%, from simulation periods 250-280, 350-380, and 450-480 (Figure 3b dashed green, dashed yellow and solid blue lines respectively), showing a tendency toward recovery. On the other hand, the delayed response in the deep NAtl is evident at depths >3000 m, where a gradual increase in the percentage change signal is observed from simulation periods 250-280 to 450-480 (Figure 3b solid blue line reaching values of up more than 50% warmer in the deep NAtl). When looking at the vertical section at the end of the Extension phase (Figure 3e), our results suggest significant changes of up to 20% and 50% warmer in the mesopelagic and deep NAtl respectively. It is important to highlight that the warming signal seems to be stronger in low-latitude regions, suggesting very long recovery timescales in the deepest domains (>3,000 m). Conversely, there is a gap in terms of significant differences in the lower mesopelagic and most of the bathypelagic domain (1,000–3,000 m; Figure 3e) between 40 and 60°N, which suggests shorter Trec values in this zone outside the timeframe of our simulations.

The delayed climate change onset (i.e., high ToDs) in the shallow NAtl (Figure 3a) and especially between 10 and 30°N as well as poleward of 50°N (Figure 3c) indicates, respectively, the subsurface water isolation in the NAtl subtropics (Figure S8) and a relatively smaller anthropogenic signal when compared to the natural variability of Temperature at temperate and subarctic latitudes. This highlights the tight natural coupling between atmospheric variability, heat exchange, and gyre circulation. Additionally, our simulation yields maximum ToD values within the thermocline zone (Figures 3a and 3c), suggesting that this region can be understood as a buffer zone in terms of seawater warming. Here, a sustained long-term anthropogenic perturbation greater than in any other region is needed before an evident climate change signal can be detected. A recent study by Hameau et al. (2019) using a different model (CESM) focused on changes within the thermocline (200–600 m) under RCP 8.5 (Representative Concentration Pathways) future scenario also suggested delayed ToD for Temperature around ∼20°N by the end of the century within the thermocline domain, which is consistent with our results. Similarly, Hameau et al. (2019) also state that this pattern is characteristic of a climate change buffer zone, influenced either by high natural variability or inhibited anthropogenic response or even a combination of both.

In contrast, despite delays in Temperature ToD at the domains described above, our results suggest that changes in the interior NAtl can occur as early as 40 years in our scenario of rapid atmospheric warming. Below the thermocline, the uniformly lower ToD values (Figures 3a and 3c) indicate how sensitive the mesopelagic and deep NAtl zones are and how early global warming can have an impact on their ecosystems relative to the surface and subsurface layers. Furthermore, our results show that the narrowest ToD spread is simulated in the mesopelagic and upper bathypelagic zone, highlighting their stable environmental conditions (i.e., narrow envelopes of natural variability) and, consequently, their susceptibility to changes in Temperature compared to other regions of the NAtl interior. Our results align with Brito-Morales et al. (2020), who conducted a study on the horizontal climate velocity concept focusing on the projected ocean temperature changes under different RCP scenarios (i.e., the horizontal extension of a 1°C change over time [km yr^{-1}]). Under RCP 2.6, their results suggest that temperature-induced climate velocities for the mesopelagic global ocean will occur 7 times faster than at the surface if compared to contemporary climate, whereas under RCP 8.5 it can be >20 times as fast. This suggests that mitigation strategies implemented to reduce atmospheric CO_2 might only be effective in lessening climate change effects in surface waters, with limited to no impact in deep ocean recoveries and direct consequences for deep-ocean life.

For most of the NAtl domains, our analyses show that the persistence of the warming signal is an indication of very slow recoveries within the time span of our simulation toward PI levels (Figures 3a and 3d). During Ramp-up, the AMOC strength is reduced, and the NADW shallows (Figures 1e and S4). In our model, the strength and volume of NADW formation predominantly control Temperature fluctuations in the upper 3,000 m whereas both the vertical extensions of NADW and AABW cells contribute to the emergence and recovery of anthropogenic signals >3,000 m. We note that changes occurring in the South Atlantic and the Southern Ocean can also play an additional role in the redistribution of heat and its exchange at intermediate layers of the NAtl once the AMOC regains its strength. Our projected low Trec at both the deepest domains of the NAtl (4,500–5,000 m) and the

surface layer (<200 m) suggests that the former can be attributed to a thermohaline recovery signal brought by AABW (Figure S4) and the latter to a recovery in subsurface levels due to, for example, restructuring of deep ocean water masses following atmospheric readjustment (Figure 3a and Animation S1).

3.2. Dissolved Oxygen (DO) and Apparent Oxygen Utilization (AOU)

After model year 180, our results for the mean state of DO evolution indicate an apparent oxygenation trend between 500 and 1,500 m depth for the tropical and subtropical domains (Figures 2c and 2h), with the shallowing of the oxygen isolines. Between 2,000 and 3,000 m, however, a decrease with respect to PI levels is observed, with DO levels rebounding both at the tropical and subtropical domains around model year 350 (see SI Animation S3 for the evolution of ΔDO over different depth layers). The evolution of DO levels at higher latitudes (Figure 2m) shows a generalized decrease relative to the PI period. A sustained vertical expansion of the subpolar minimum at ∼500 m is projected and lasts the entire Ramp-down phase. In the bathypelagic domain (3,000–4,000 m), a decrease in mean DO state happens later, after the CO_2 peak (model year ∼170), with a sustained decrease even after the end of the experiment. At the abyssopelagic subpolar domain (>4,000 m) a change in the mean DO state is projected to occur even later, model year ∼300.

A generalized decrease in AOU levels is projected for both the tropical and subtropical domains (Figures 2d and 2i). Our results suggest that in the mesopelagic tropical NAtl (∼1,000 m) AOU levels are lowered by up to 60 μmol kg^{-1}. The isoline of 40 μmol kg^{-1} starts shallowing within the Ramp-down (model year ∼200) and is found at a shallower position in the subtropical domain compared to the tropical domain. In the subpolar NAtl (Figure 2n), AOU values are relatively low due to the highly oxygenated young water masses originating at subduction zones. Two regions are marked by projected decreases of 20 μmol kg^{-1} at model year 160, the subsurface (∼200 m) and the upper bathypelagic (1,500–2,000 m). In the abyssopelagic subpolar NAtl, an increase of 20 μmol kg^{-1} in AOU is observed with respect to PI levels, indicating an increase in the age of water masses following the slowdown of the AMOC, corroborating the projected changes in ideal water mass age (Figure S8)

Our results indicate overall deoxygenation in the upper layers of the NAtl throughout the Ramp-up phase, with greater ToD values than in the deeper layers, which reflect the wider envelopes associated with the high interannual variability due to the efficient air-sea gas exchange and biological processes within the mixed layer. Our results are consistent with Hameau et al. (2019) and Tjiputra et al. (2018a), who also suggest relatively higher ToD timescales for DO in shallower domains of the NAtl (<600 m), except for the regions between the center of the subtropical gyre and the western side of the basin. In the NAtl interior, the simulated ToD values decrease, indicating the stable mesopelagic and bathypelagic environments with respect to DO. Interestingly, departures within the upper layers were generally associated with a deoxygenation signal related to warming, whereas for the mesopelagic and upper bathypelagic (500–2,000 m) this was not the case. In the tropics and subtropics, the almost mirrored patterns of DO and AOU in Figures 2c and 2d and 2h-2i in the upper 2,000 m indicate that the large-scale recovery of DO is mostly driven by a rebound in AOU and biological activity. In the subpolar NAtl (Figures 2m and 2n) however, while DO levels tend to recover toward PI levels, an undershoot in AOU with respect to PI levels remains, suggesting that the DO recovery is also influenced by an increase in oxygen saturation levels.

Along the western NAtl meridional section, ToD for DO (Figure 4a) and AOU (Figure S9) indicate an overall consistent and decreasing pattern with narrowing uncertainties at depth until the mid-bathypelagic (2,000 m). Subsurface DO and AOU ToD estimates show values of 100 ± 30 years, whereas at 2,000 m values are ∼45 ± 15 years. The narrowing of the DO ToD spread reflects the relatively stable mesopelagic and deep NAtl with respect to temporal fluctuations in DO. Additionally, a feature of particularly high DO ToD values is observed at 20–30°N between 2,000 and 3,000 m (Figure 4c), suggesting a highly delayed anthropogenic signal which matches the pattern observed in Figure 3a for Temperature. These delays may be indicative of the relatively weak influence of the NADW water mass in this region and/or delay in the changes of horizontal circulation patterns.

Our analyses suggest that projected departures can also be associated with an increase in DO that is closely linked to reduced AOU at depth. The relationship between an AOU undershoot (i.e., transition from surplus to deficit conditions relative to PI) and a DO overshoot (i.e., a transition from deficit to excess conditions relative to PI) can be seen in (a) the profiles of DO and AOU Trec, where a peak of delayed Trec in AOU (between 700 and

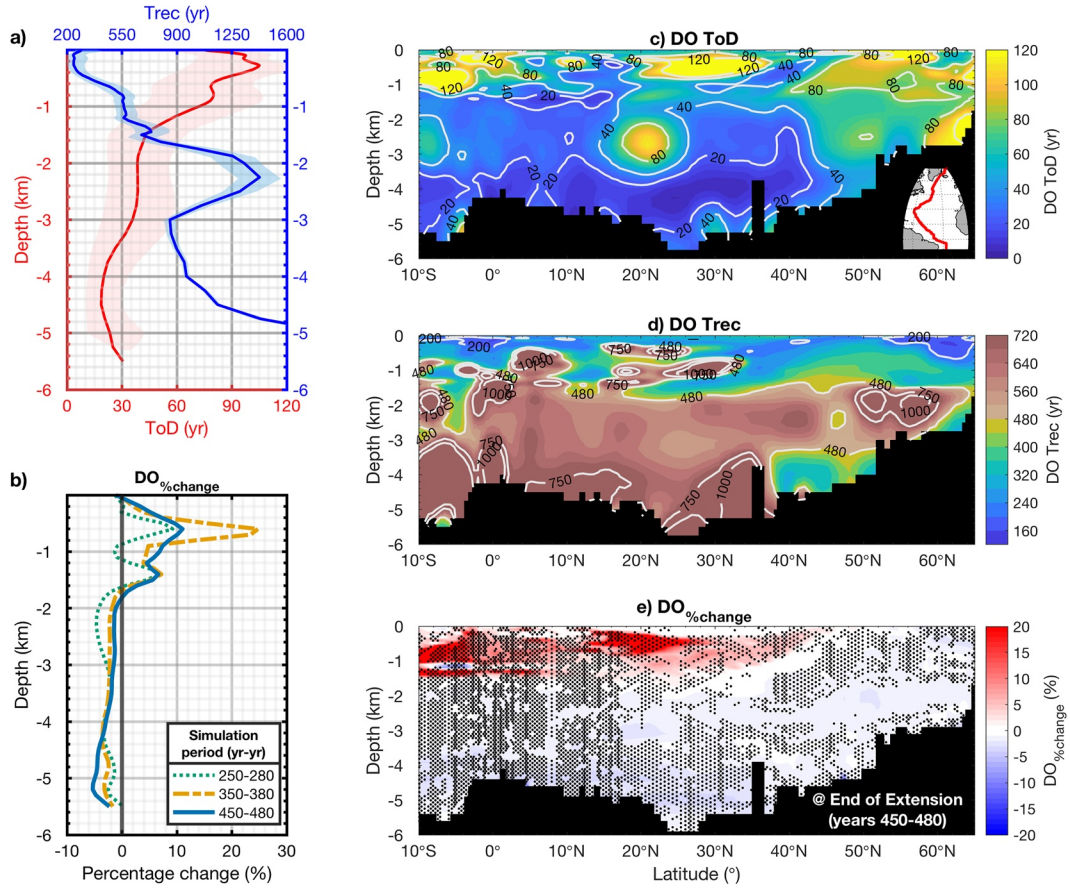

Figure 4. As in Figure 3, but for Dissolved Oxygen (DO).

1,500 m) is lying just above the peak of delayed Trec for DO (between 1,800 and 2,400 m; Figure S10) and (b) the mean DO and AOU percentage change profiles across all the different simulation periods from the subsurface down to 1,500 m (Figures 4b and S9b), which clearly show sustained positive (negative) changes for DO (AOU).

Between 1,500 and 3,000 m depth, the magnitude of changes in DO decreases chronologically after model year 250. The magnitude of AOU percentage change for this domain also shows a recovery trend toward PI levels. In the upper 1,500 m, the delay in DO recovery is evident, with DO percentage change values increasing after model year 250 toward model year 380 before showing a sustained decrease, even though not reaching PI levels at the end of the simulation. This indicates the out-of-phase recoveries, with rebounds back to PI levels expected sooner for deeper domains than at the subsurface. In fact, AOU percentage change levels for the upper 1,500 m did not show a tendency toward PI levels (Figure S9b, profiles far from 0% change vertical line) and remained at negative values.

The combination of a DO overshoot and a constant AOU undershoot between 1,000 and 2,000 m after mitigation indicates that the accumulation of oxygen in the mesopelagic and bathypelagic NAtl is likely a result of less oxygen utilization over time, a feature also found in other studies (Tjiputra et al., 2018a). At the Warming Hole, more specifically, observational data at intermediate depths (~1,200 m) already show a weak oxygenation trend (Oschlies et al., 2018). Overall, our simulation suggests that this effect is a direct consequence of reduced EP from the surface layers to the NAtl interior (see below Figure 6f), which creates a surplus of unutilized oxygen at depth when compared to the PI.

Furthermore, the resemblance of DO and Temperature ToD vertical profiles (Figures 3a and 4a) in the NAtl indicates that interior changes of these parameters are similarly affected by changes in interior circulation, hence watermass reorganization. This is consistent with the observed circulation-induced recent changes in NAtl oxygen (Stendardo & Gruber, 2012). When looking at the meridional sections, a feature to highlight is the relatively high

delay in terms of DO (and Temperature) ToDs, from the subsurface down to 3,000 m and between 20 and 30°N. At shallower levels (<1,500 m), this is likely associated with shifts in the depth horizon of central water masses (Figure 4c). Under rapid anthropogenic warming, NorESM1-ME tends to produce deeper formation zones for central water masses (Bentsen et al., 2013), such as the Western North Atlantic Central Water (WNACW), which receives input from the Mediterranean Overflow Water (MOW). Liu and Tanhua (2019) described that the WNACW normally occurs in the upper layer down to 1,000 m. This is consistent with our results (Figure 2), where isolines of Temperature and DO in the interior NAtl shifted down by more than 1,000 m, yielding a new depth level of ~2,000 m. At deeper levels (e.g., between 2,000 and 3,000 m), however, the delay in ToD is related to the low-ventilation character of this part of the NAtl subpolar gyre, which is demonstrated by analyzing (a) both $Temp_{tmax}$ and DO_{tmax} surfaces within the 500–2,500 m depth range against the model years in which these signals are observed (Figures S11 and S12 respectively, panels e–f), and (b) the ideal watermass age yielded by NorESM-1 ME between 20 and 30°N at 2,500 m depth along the NAtl section (Figure S8), which shows very old water mass with very low ventilation rates. Therefore, anthropogenic signals from the surface reach this domain later than other regions at the same depth level.

Trec timescales for DO increase gradually from the subsurface toward a local maximum in the bathypelagic NAtl at ~2,200 m, followed by a decrease down to 3,000 m and a subsequent increase toward the abyssal ocean (Figure 4a). In the subsurface down to the mesopelagic (1,000 m), recoveries are projected to occur within the time span of our simulation (Trec <480 years) except for two domains at the subsurface comprised between 5-10°N and 20–30°N where projected timescales of Trec seem to be at least twice as long (Figure 4d). In the bathypelagic NAtl between 2,000 and 3,000 m depth, recoveries are projected to occur no less than 1,300 model years after the start of the Anthropogenic simulation, with two high-Trec clusters, one in the equatorial region between 0 and 5°N and another in the subarctic domain between 50 and 60°N (Figure 4d). Past 3,000 m, the subsequent decrease in Trec is associated with likely recoveries within the time span of the simulation between 40 and 60°N, suggesting the AMOC is regaining its strength and the recovery of DO toward PI levels is initiated. Overall, our results indicate that both the subsurface and the very deep domains are likely to recover before the mesopelagic and bathypelagic domains, where a tongue of particularly high DO Trec values persists between 1,000 and 3,000 m.

Our results for mean DO percentage change show two contrasting domains (Figure 4b). Regions below the NAtl mixed layer (i.e., the mesopelagic between 500 and 1,000 m) experience an oxygenation trend of +10%, +25% and then returning to +10% relative to the PI levels from the end of Mitigation to middle and end of Extension phases respectively. On the other hand, deep NAtl domains experience overall deoxygenation trends. The bathypelagic between 1,500 and 2,000 m is the region with the lowest DO content, decreasing by 5% at the end of the Mitigation phase and regaining DO as the simulation evolved toward the end of Extension phase, where levels were ~2% lower than PI values. Conversely, no rebound is projected for the abyssal NAtl (see SI Animation S3), with the highest DO change of approximately −6% at the end of the simulation.

When looking at the meridional section, it is important to highlight that the oxygenation just below the mixed layer is limited to the region south of 40°N. North of 40°N, a slight but significant trend of deoxygenation is simulated (up to −5% compared to PI levels, Figure 4e). Additionally, the gap in terms of significant differences in the bathypelagic NAtl (1,000–3,000 m) between 40 and 60°N suggests eventual recoveries in this zone outside the timeframe of our simulation similar to the pattern for Temperature (Figure 3e).

South of 40°N in the lower mesopelagic (800–1,000 m) there are still domains where significantly strong oxygenation trends of +20% can be seen, with the opposite trend in AOU for the same domain (Figure S9e). Furthermore, the depth range of these domains increases southwards, reflecting the strong effect of remineralization rates in low and mid-latitude upper ocean water masses of the South Atlantic on DO levels of the NAtl interior. This shows that, under our simulation, NorESM1-ME yields recovery timescales for the South Atlantic that are significantly longer when compared to the NAtl, highlighting that DO recoveries in the low to mid-latitude domains of the NAtl interior also rely on the readjustment timescales of water masses from the South Atlantic. Between 2,000 and 3,000 m, while the AOU signal shows overall recoveries toward PI levels in the NAtl within our simulation period (Figure S9d), DO levels show no recovery (Figure 4d). This indicates that, even though there was a recovery with respect to the amount of oxygen being consumed for remineralization, the major factor impeding DO recovery within this depth range is the solubility effect of Temperature prevailing in the South Atlantic, which reduces DO levels at depth even after the Extension phase (Figures 4b and 4e).

3.3. pH and Calcite Saturation State (Ω_c)

The evolution of the mean pH vertical profile indicates that the mesopelagic and upper bathypelagic NAtl domains (500–1,500 m) will experience pH values as low as 7.6 for a sustained period. A decrease of 0.3 units with respect to the mean PI pH state is projected for the tropical domain (Figure 2b, ~2,000 m), whereas in the subtropical and subpolar domains, the decrease is even stronger and its peak coincides with the peak of CO_{2atm} (0.5 and 0.6 units, Figure 2g,2l, respectively). In the tropical domain, the strongest acidification signal (~500 m) persists throughout Ramp-down (Figure 2b). The progradation of the acidification signal is also stronger at depth in high latitudes (see SI Animation S2 for the evolution of ΔpH over different depth layers). In the subpolar NAtl, even though the signal is relatively short-lived compared to the other latitudinal domains, it penetrates through most of the water column (up to 3,000 m), as opposed to being confined in the upper 1,000 m. As CO_{2atm} increases during Ramp-up, the oceanic uptake of excess CO_2 increases, leading to the higher surface dissolved inorganic carbon concentration (DIC, Figure S13, and Animation S6) and consequently lower pH. Subsequently, as CO_{2atm} levels decline during Ramp-down, the ocean starts outgassing, and surface pH returns to the PI level. The response of interior pH is more complex as the ocean overturning transports low-pH watermasses into the interior at a much slower time scale than the evolution of CO_{2atm}. We also note that, while increasing DIC is the main driver of acidification signals, changes in other parameters such as temperature and alkalinity also affect ocean pH (Fransner et al., 2022).

The evolution of the mean Ω_c vertical profile shows that minimum values reach their shallowest position roughly during model year 140 for all latitudinal domains in the NAtl, coinciding with the peak of CO_{2atm} (Figure 2e,2j,2o). A low value of Ω_c persists throughout the entire water column at both the tropical and subtropical NAtl during the Mitigation phase (i.e., Ramp-down, model years 140–280). This highlights the time lag between the implementation of mitigation measures and the actual response in the interior ocean. Furthermore, it is in the subpolar domain, that conditions favoring calcite dissolution are projected (Figure 2o). Ω_c values < 1 start to arise before the peak of $CO_{2atm,}$ in the deep ocean (model year 100, 3,000 m depth), with the dissolution signal intensifying and expanding to shallower depths throughout the Ramp-up phase.

The onset of climate change for Ω_c can be detected throughout the water column in less than 50 years (Figures 5a and 5c), correlating tightly with patterns from the pH ToD profile (Figure S14). The subsurface zone (0–500 m) shows the earliest departures (10 ± 5 years) due to the decrease in pH as a result of enhanced CO_2 uptake from the atmosphere. In the mesopelagic and upper bathypelagic NAtl (500–1,500 m) a relatively higher Ω_c ToD is simulated (50 ± 15 years), forming a buffer zone for ocean acidification. This part of the NAtl is mainly influenced by two major clusters of relatively high ToD values, between 15 and 30°N at ~1,000 m and between 45 and 60°N at 1,500 m depth (Figure 5c). Ω_c ToD decreases gradually between 1,500 and 3,000 m, reaching practically homogeneous values within the 2,500–3,500 m depth range that are similar to values found at the very surface (10 ± 5 years). This shows not only the connectivity of this zone via deep ocean ventilation but also a very stable environment that is prone to change. In the abyssal NAtl, however, the results from our simulation show a gradual increase in Ω_c ToD values (Figures 5a and 5c), unlike what is observed for Temperature, DO, and pH (Figures 3a, 4a and S14a, respectively). Figure 5b shows that the period with the highest percentage change of Ω_c in the NAtl is the end of the Mitigation phase, where saturation states decreased by more than 25% in the entire bathypelagic (1,000–3,000 m) relative to PI levels. These negative changes are attenuated over time, with absolute negative changes decreasing from approximately 15% to <5% from the middle to the end of the Extension phase, respectively.

Decreases in Ω_c peaked at the end of Mitigation (model years 250–280), with the volume-weighted profile for the whole NAtl from 0 to 65°N (Figure 5b) showing saturation states 25% lower than PI levels for the upper bathypelagic domain (1,000–3,000 m). Even though decreases are projected, results shown in Figure 2 suggest that large parts of the NAtl will remain oversaturated with calcite, as conditions close to undersaturation are simulated and persist throughout Ramp-down between, for example, 500–1,000 m (Figure 2e). ToD results in Figure 5c suggest delays in the upper 1,000 m south of 30°N, which might be linked to lower EP and therefore, lower remineralization at this depth curbing a further increase in acidity. The slight delay in the NADW domain at 1,500 m (30–60°N) may suggest that a reduction in Ω_c due to invasion of anthropogenic carbon is buffered by heat uptake.

Furthermore, in the lower mesopelagic (~1,000 m), the northward flow is reduced during Ramp-up (see stream function values in Figure S4). The delay in ToDs for both pH and Ω_c in the region (Figures S14c and 5c) can

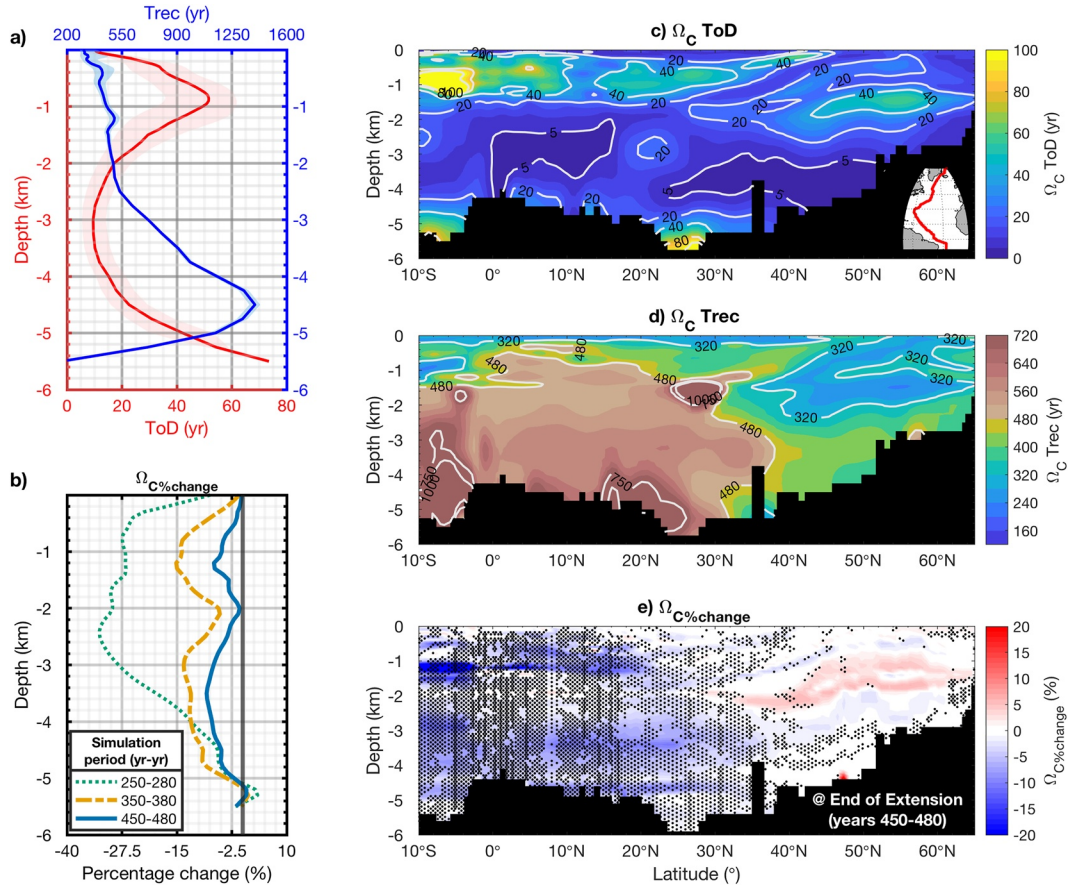

Figure 5. As in Figure 3, but for Calcite saturation state (Ω_c).

also be associated with (a) a weakened northward advection of DIC-rich watermass from South Atlantic and (b) lowered EP, which reduces DIC production from remineralization, buffering acidification rates and changes in Ω_c. This also suggests that the interplay between northward transports from the South Atlantic and the time when the AMOC slows down at subduction zones can also affect the decrease and the spread of the low Ω_c signal in the mesopelagic and upper bathypelagic NAtl (500–2,000 m). This gradual change toward a weaker AMOC may create latency which allows for a buffering effect associated with penetration of a relatively high (i.e., unaltered) pH signal from the south at intermediate depths.

At the very bottom, one of the main factors contributing to Ω_c levels holding up (~4,000 m) despite pH levels changing relatively fast (Figure S14c), is the warming signal that reaches the abyssal domain (Figures 3a and 5a), which counteracts the effect that acidification has on Ω_c (i.e., warming increases Ω_c whereas lower pH is associated with lower Ω_c). Therefore, the net effect is reflected as very small changes in Ω_c over time, if compared to the projected changes in Temperature, pH, and DO, leading to longer ToD timescales in the abyssal domain. We highlight that understanding these latent relationships along with the opposing transport effects occurring at intermediate and abyssal depths is crucial to projecting more precisely not only the contributions of unaltered volumes from the South Atlantic (Krumhardt et al., 2020), which in turn are able to curb the acidity signal brought by NADW, but also improve the estimates of ToD timescales. This dynamical feature could be model-dependent and future analysis using different model systems would be valuable (see section '3.5 Limitations and Recommendations'). Furthermore, we note that conjunction of different processes can be responsible for the observed delayed departures. We emphasize that more studies are needed to better constrain the different physical and biogeochemical drivers on the projected Ω_c changes under scenarios of anthropogenic forcing.

Unlike what has been observed for the departure timescales associated with Temperature and DO, ToD values for Ω_c did not form an apparent cluster of delayed departures in the domain characterized by MOW influence (Figure 5c, ~30°N). This may be related biases from NorESM's representation of the MOW in the deep NAtl

(Bentsen et al., 2013), suggesting that anthropogenic disturbances altering the Ω_c signal in the Mediterranean are readily cascading through the mid-latitude zones of central water masses and resulting in early ToDs.

While a localized cluster of delayed Trec cannot be observed for Temperature at 30°N (i.e., late recoveries seem to be widespread over the interior NAtl), our results revealed the presence of delayed Trec clusters for both DO and Ω_c (Figures 4 and 5d). The depth range of these clusters differs, with the DO cluster appearing at a shallower position (~1,000 m) compared with that of Ω_c (~1,500 m). This disparity indepth horizon may be partially attributed to local increases in biological activity as the AMOC regains strength and the mixed layer deepens once again (Figure S3), which stimulates EP (Figure 6d, transect at 30°N passing through cluster of no departures surrounded by very early recoveries), and initially induces high remineralization at intermediate levels (i.e., decreasing DO and sustaining the delay in DO recovery). The local rebound in remineralization leads to a subsequent injection of DIC at deeper levels (Figure S13 and Animation S6), therefore decreasing overall pH and sustaining a net decrease in Ω_c for longer.

Lower Ω_c Trec values (up to 320 years), were characteristic of the surface, between 0 and 250 m depth, and throughout the mesopelagic down to 2,500 m (Figures 5a and 5d). This shows that recoveries with respect to Ω_c are unlikely during the simulated Mitigation phase and are only observed some 50 years into the Extension phase. When the extent of recovery along the meridional section is examined, a distinct separation is seen at the latitude of 35°N. Domains north of 35°N showed recoveries within the last 30 years of the simulation (Figure 5d) and even some minor Ω_c overshoots associated with insignificant differences between 1,000 and 2,000 m off Newfoundland (up to +5%), encompassing most of the Labrador Sea (Figure 5e and Animation S5). This may be a signal related to a local rebound in pH as well as contributions of pH-recovered surface waters, brought by the northernmost NADW subduction cell as south as 35°N, while Temperatures remained relatively high throughout the simulation.

South of 35°N, relatively late Trec values were obtained for most of the subsurface, mesopelagic, and deep NAtl domains with estimates no lower than 500 years and even higher southwards (Figure 5d). It is important to highlight the presence of a particularly high Ω_c Trec region observed between 2,000 and 3,000 m depth around 20°N, where Trec values are greater than 1,000 years. This region coincides with the zone of relatively low-ventilation timescales. Southwards, significant undershoots are still present and are pronounced in domains that are influenced by intermediate and potentially deep water masses from the South Atlantic. Regions encompassed by the meridional section show an overall significant decrease of up to −10% even at the end of the Extension phase south of 20°N, with a localized minimum of up to −20% at around 1,000 m depth. This suggests that the anthropogenic disturbance is still propagating southwards within the low latitudes as a persistent decrease in pH as well as DIC excess, which is reflected in the NAtl interior on the Ω_c signal (Figures 5e and S14e).

Overall, changes in projected Ω_c appear predominantly determined by the invasion of anthropogenic carbon and to some extent buffered by ocean warming and/or changes in EP and DIC transport throughout the interior following lagged responses by the AMOC. The anthropogenic DIC invasion predominantly controls the evolution of Ω_c, which is reflected by the spatial patterns seen between Figures 2e-2j-2o and S13b,c,d. The anthropogenic carbon enters NADW through the Nordic and Labrador Seas before propagating southward through the return flow of overturning circulation (see AMOC stream function Figure S4; Fransner et al., 2022; Tjiputra, Assmann, & Heinze, 2010). This is why the domains strongly influenced by NADW have the lowest Trec (Figure 5d) following the end of Ramp-down, as watermasses now equilibrated once again with PI CO_2 levels start entering the deep ocean. Tropical and subtropical deep-water domains (>3,000 m) will also eventually recover but only after excess DIC that accumulated from earlier is redistributed, as shown in Figure S13b,c (see also Animation S6).

3.4. Export Production (EP)

Figures 6a and 6b show that an expansion of the low EP area is noticeable in the subtropical gyre and the western part of the NAtl, over the Sargasso Sea domain. Conversely, at higher latitudes, there has been an increase north of 45°N between 40 and 45°W, which coincides with the latitudes of occurrence of the Warming Hole. Eastwards, decreases are also noticeable, with widespread decreases along the European shelf (45°N,10°W) as well as a significant reduction over the Canary upwelling system (22°N,18°W). However, some patches of localized increase in EP were also observed, especially in parts of the Irminger Sea and the domain from the Reykjanes Ridge to the Azores, which are associated with relatively later ToD values (>250 model years, Figure 6c). There is little variation in both zonally-averaged EP ToD and Trec, indicating that, at domains where departures were observed, significant changes in EP will occur no later than ~10 years into the Mitigation phase with a general trend toward earlier departures in higher latitudes (Figures 6c and 6e).

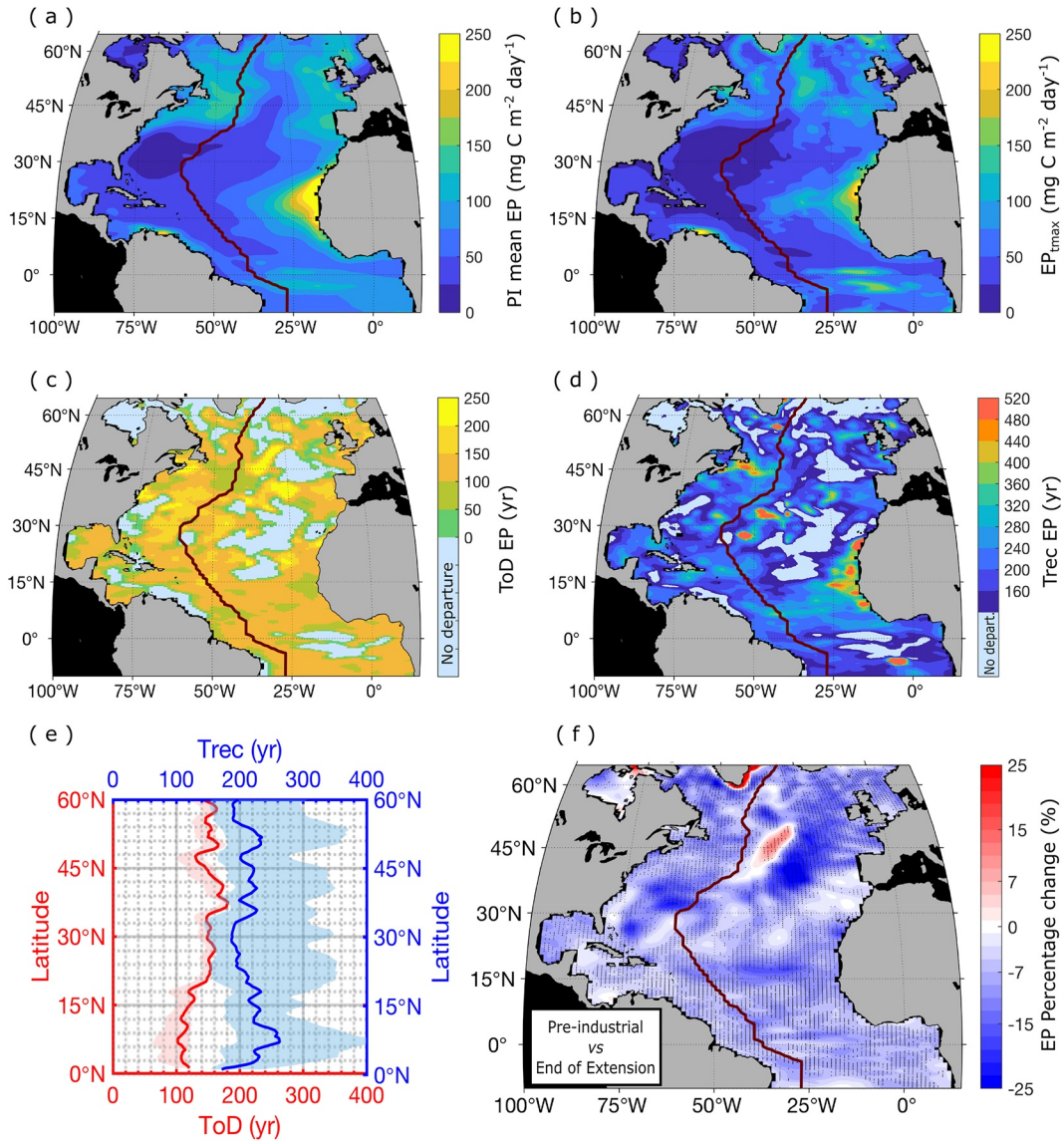

Figure 6. NorESM1-ME maps of Export Production (i.e., Particulate Organic Carbon export at 100 m depth) related variables. (a) Pre-industrial mean spatial distribution [mg C m^{-2} day^{-1}]; (b) at tmax [mg C m^{-2} day^{-1}]; (c) Time of Departure (ToD) and (d) Time of Recovery; (e) North Atlantic (0–60°N) zonally-averaged area-weighted mean EP ToD and Trec (yr) and (f) mean percentage change (%) at the end of the Extension phase, where stippling indicates regions of significant differences. The timescale estimates are based on an envelope of 2 standard deviations with light blue areas showing regions of no departure in panels (c) and (d). All year units are model years since the start of the simulation. Shading around solid lines in panel (e) represent uncertainty range estimated using different natural variability envelopes (see Section 2.4).

The simulated EP ToD values mostly ranged between 100 and 150 years (Figures 6c and 6e), or no departures at all. When zonally averaged, EP ToD revealed values of relatively early departures toward the Equator and patches of 'no departure' predominantly throughout the eastern NAtl north of 15°N and in higher latitudes (>60°N; Figure 6c). Late departures are found in regions of transition between the subtropical and the subpolar gyres (~180 years) and coincide with the regions of highest natural variability, such as the Labrador Sea and the Warming Hole area.

Overall EP Trec estimates reveal a homogeneous meridional distribution with mean values of ~200 years, suggesting that recovery timescales are projected to occur toward the end of the Mitigation phase. A relative increase toward lower latitudes is projected, but Trec values remain <250 years, indicating delayed recoveries in this region. This is mainly attributed to the high natural envelope simulated both at the Canary and western Afri-

can upwelling regions (Figure 6d). Other exceptions include the Azores and the Grand Banks off Newfoundland, where Trec estimates were outside of our simulation period (>480 years).

Compared to the PI, EP at the end of the Mitigation phase is projected to decrease between −20% and −25%, except for a region encompassing the western part of the Irminger Sea and the domain from the Reykjanes Ridge to the Azores, where percentage changes exceeded +25%, coinciding with the Warming Hole region (Figure S7). Both the positive and the negative changes gradually decrease over time in terms of magnitude and spatial extent. At the end of the Extension phase, our results indicated that the NAtl domain becomes largely less productive with an overall decrease in EP by up to −20% in parts of the subtropics. However, positive changes over the Azores ridge and the western Irminger Sea remain, with EP values of up to +15% higher than PI, showing some localized increase over the Warming Hole region (Figure 6f).

The last 30 model years of the simulation reveal a scenario of predominant decrease in EP except for the Warming Hole area in the subpolar region, where trends toward cooling, oxygenation, and increased EP were detected at the end of the simulation. The increases in DO and EP signals seem to result from enhanced instability in the water column caused by the decrease in Temperature, which deepens the mixed layer depth (MLD, Figure S3), favoring productive regimes as well as enhanced ventilation.

3.5. Limitations and Recommendations

NorESM1-ME model-dependent biases described in Section 2.1 are likely to affect the magnitude and rate of change of the variables analyzed in our study, however, the overall direction of change during Ramp-up and Ramp-down is generally consistent with other models. For example, the propagation of anthropogenic warming in the subpolar domains is evident throughout Ramp-up in other models, with faster changes in the interior ocean (see SI for a more detailed comparison). Given that NorESM1-ME simulates an anomalously too strong overturning strength, there could be biases in our simulated timescales (ToD and Trec) when compared to the real ocean. Furthermore, it is evident that spatial patterns vary between models since different ESMs simulate differently both the interior watermass structures and pathways (Langehaug et al., 2012). Nevertheless, our North Atlantic ToD pattern for Temperature exhibits similar features at depth as the study by Silvy et al. (2020), who used an ensemble of CMIP5 ESMs under the RCP 8.5 scenario (e.g., low ToD at ∼40°N from the surface down to 1,000 m as well as 2,000–3,000 m depth in low latitudes, due to the relatively weak background natural variability leading to earlier emergence of anthropogenic signals).

In the abyssal, a previous study suggests the NorESM1-ME ventilation by AABW is relatively weak (Bentsen et al., 2013). The changes in this region are likely not, or weakly, related to forcing from the surface. Therefore, the timescales we obtain from the abyssal NAtl are likely to be affected by watermass restructuring rather than due to changes in AMOC strength. Yet the lack of long-term observational data in the interior ocean makes it difficult to carry out model validation to discern how the anthropogenic signal affects the interior ocean circulation and subsequently changes interior watermass structures. Long-term sustained observations are therefore undoubtedly needed (Silvy et al., 2020) and efforts such as the Deep Argo Mission are underway to fill the gap of long-term observational timeseries data in the oceans interior over the anthropogenic era. Additionally, we highlight that assessing the sensitivity of ToD and Trec to the simulated water mass structures and different physical model parametrizations is also an important follow-up topic. Future studies are needed to not only better constrain anthropogenically-induced variability in the interior ocean but also better understand how model-dependent features deviate from the real ocean.

Biases in our analyses can also arise from uncertainties linked to biogeochemical parameterizations in the model. For example, the interior oxygen consumption during organic matter remineralization is highly simplified and based on a constant remineralization rate. Studies have indicated that Temperature plays a significant role in DO consumption at depth (Brewer & Peltzer, 2016, 2017), which could consequently impact oxygen projections under future climate change. The sensitivity of our timescale analyses to different biogeochemical parametrizations remains unexplored and could be investigated in further studies. Understanding how changes in horizontal circulation mediate projected timescales is also key, however, advective terms of, for example, oxygen sources and sinks are required, which the most current models, unfortunately, do not produce, highlighting the need for further studies.

Improving how EP is represented in the models is valuable to understand whether the features observed here arise from adopting a relatively shallow layer, where productivity is confined to the first 100 m and the recycling of organic matter is not mediated by an explicit microbial loop or warming. Furthermore, a more robust representation of the lower trophic ecosystem processes and the adoption of our method using other ESMs can improve our understanding of any simulated counterintuitive patterns (e.g., the oxygen overshoot in the meso- and bathypelagic domains followed by warming and the Warming Hole region characterized by cooling and enhanced EP). Such an exercise can help us determine, for example, whether the oxygen overshoot detected here is a model caveat or an actual indication of the solubility effect being surpassed by biological activity and/or the effect of the redistribution of PI DO due to changes in the circulation under extreme climate change. Moreover, the use of more realistic climate change and mitigation scenarios in such studies, for example, SSP5-3.4, can ultimately help shed new light on where the threshold lies in terms of the amount of change that is necessary for the solubility effect to become less important in controlling DO levels in the NAtl interior.

In addition to the model-specific biases discussed above, there is the uncertainty arising from different model systems. For example, even though the anthropogenic acidification signal seems to be weaker and less sustained (i.e., it does not last as long) in NorESM1-ME (Figure 2g) when compared to CESM2 (Figure S17d), it penetrates deeper in the subtropical domain. More model simulations from CDRMIP are emerging, and the analyses conducted here could be implemented in a multi-model framework. Although outputs from the CMIP6 models often do not include all the variables analyzed in this study, we present in Section 3 of our SI a comparison between NorESM1-ME (CMIP5) and the available CMIP6 models (NorESM2-LM; [Tjiputra et al., 2020]); CanESM5 (Swart et al., 2019); CESM2 (Danabasoglu et al., 2020); GFDL-ESM4 (Dunne et al., 2020); CNRM-ESM2-1 (Séférian et al., 2019); Figures S15-19) in terms of strength and penetration of anthropogenic forcing over different latitudinal domains and the evolution of EP at 100 m depth across those different models (Figure S5). We note, however, that CMIP6 models consist of shorter runs when compared to NorESM1-ME, which, in terms of Extension Phase, remains the longest model running the CO_2 ramp scenario (total run of 480 years, while models from CMIP6 stop their runs before or at 400 years).

4. Summary and Conclusions

Despite applying symmetrical forcing (i.e., a CO_2 Ramp-up of $+1\%\ yr^{-1}$ followed by a CO_2 Ramp-down of $-1\%\ yr^{-1}$), our study reveals that the responses observed in the interior NAtl in terms of physical and biogeochemical drivers were asymmetric, with strong spatial variations that remained even after allowing for stabilization over the Extension phase. Our study highlights that vast regions in the interior NAtl, especially the meso and bathypelagic, tend to respond to anthropogenic forcing significantly earlier than domains in the subsurface. It is also in these regions of early departure that recovery timescales are mostly affected, meaning that in regions of relatively rapid change the recovery is even slower.

When looking at individual parameters, Temperature data revealed overall very long recovery timescales in the interior NAtl toward PI levels. At the end of the experiment, the mesopelagic and bathypelagic regions displayed modest cooling in response to decreased anthropogenic forcing but remained 15% warmer than the PI on average. Conversely, instead of cooling, NorESM1-ME simulation data suggest that Temperature in the domains of the deep NAtl were progressively warm throughout all the simulation phases. This suggests that domains in the South Atlantic and the Southern Ocean accumulated heat as the AMOC slowed down over Ramp-up. Once the AMOC regained some of its strength, this heat surplus started to be exchanged across the Atlantic, potentially affecting readjustment timescales over the entire deep NAtl as far as 50°N (Figure S3, for the evolution of NorESM1-ME heat content and MLD in different latitudinal domains).

With respect to oxygen, our data suggest a pattern of rather a counterintuitive oxygenation despite the anthropogenic warming in the mesopelagic and upper bathypelagic NAtl. This oxygen overshoot is linked to a decrease in biological remineralization, which is caused by a decrease in export production from the surface layers. This ultimately translates into a reduction in the amount of organic matter exported to and remineralized in the ocean interior, creating a surplus of unutilized oxygen relative to the PI. Regarding Ω_c, our simulation suggests that departure timescales in the upper mesopelagic NAtl are closely linked to changes in pH and the invasion of anthropogenic carbon mediated by the gradual attenuation of the AMOC. This interplay allows for a potential short-lived dominant buffering with respect to the penetration of a relatively high-pH signal from the south at

intermediate depths. This buffering effect, however, seems to be stronger in domains influenced by volume contributions from the South Atlantic. Further investigations on how these opposing transports, which counteract the acidity signal from NADW, affect timescales of climate change are crucial to improve our understanding of how relatively unaltered volumes from the South Atlantic have an impact on ToD timescales in the mesopelagic NAtl. We emphasize that this dynamical interplay could be a model-dependent feature and further studies using different models would be valuable.

Here we show that for variables that revealed recoveries within the timeframe of the simulation, the recovery timescales in the NAtl interior are out of phase (i.e., not concurrent). For example, the layered structure of delayed Trec values for DO and Ω_c at mid-latitudes reveals that recovery signals may be associated with upper-ocean biogeochemical changes (e.g., local increase in EP), while deeper than 1,500 m variations in ventilation timescales may also play a role in the out-of-phase recovery. Our results suggest interior water mass restructuring can be important in controlling the recovery of Ω_c in mid-latitudes of the meso- and bathypelagic NAtl. Further studies focused on the impacts of circulation changes that affect the formation of mid-latitude water masses are needed to better understand the impacts on the biogeochemistry of the North Atlantic interior under climate change.

We highlight that future studies focused on the relationship between AMOC strength, changes in ocean biogeochemistry, and their effects on ToD and Trec timescales in the deep ocean are needed to better understand how these properties are linked and how they translate into exposure horizons beyond which significant changes in marine assemblages are expected. The existing studies that have modeled timing of climate change emergence (i.e., ToD), as well as the timing of exposure to conditions beyond niche limits, are scarce for marine species, mostly confined to the epipelagic zone and have focused on changes in terms of Temperature. We currently lack more integrative approaches involving the covarying and synergistic effects of biogeochemical variables on ecosystem function, which can constrain species' ranges and their tolerance to climate change scenarios even more (Coll et al., 2020; Trisos et al., 2020).

To conclude, we reiterate that it is time for the community to start focusing not just on changes to the marine environment in the epipelagic zone given how vast, biogeochemically active, and interconnected the various domains of the interior NAtl are. The results shown here come from a single model and it would be invaluable to test the robustness of our results using other models. As more model simulations from CDRMIP become available, we recommend further studies to assess the sensitivity of our results in other models. Holistic modeling exercises on how covarying shifts in biogeochemical drivers can be used as proxies for changes in deep-ocean marine assemblages are key to better inform policymaking. Such studies can aid in our understanding of how exposure times can affect carbon and nutrient recycling at depth, water mass restructuring, as well as species distribution and ultimately help better project the consequences of climate change scenarios for the mesopelagic and deep ocean.

Data Availability Statement

The NorESM1-ME ramp-up simulation output is publicly available at the CMIP5 repository: https://esgf-data.dkrz.de/projects/esgf-dkrz/. Fully coupled ramp-down and extension simulations are long-term archived at the NorStore Research Data Archive and can be accessed under https://doi.org/10.11582/2018.00011. All the scripts used to analyse output data from NorESM1-ME, calculate timescale variables, perform percentage change significance tests and produce high-resolution images can be found in the following online repository for easy and user-friendly access: https://github.com/LeoBertini/NorESM_ramp_study.git. The code is written in MATLAB 2018b. A brief explanation of all the scripts is given in the 'Readme.md' file.

Acknowledgments
We acknowledge the Norwegian Research Council funded projects CE2COAST (№ 318477) and COLUMBIA (№ 275268) and the EU Horizon 2020 research and innovation programme under grant agreement № 869357 (project OceanNETs). This study has been carried out as part of the IMBRSea Erasmus+: Erasmus Mundus Joint Master's Degree (EMJMD) Programme and supported by an EMJMD Scholarship, under the EU Grant Agreement № 2016-2280. We would also like to thank all the anonymous reviewers for their comments and contributions, which have greatly improved our manuscript.

References

Assmann, K., Bentsen, M., Heinze, C., & Segschneider, J. (2010). An isopycnic ocean carbon cycle model. *Geoscientific Model Development*, *3*, 143–167. https://doi.org/10.5194/gmd-3-143-2010

Baillon, S., Hamel, J.-F., Wareham, V. E., & Mercier, A. (2012). Deep cold-water corals as nurseries for fish larvae. *Frontiers in Ecology and the Environment*, *10*(7), 351–356. https://doi.org/10.1890/120022

Bentsen, M., Bethke, I., Debernard, J., Iversen, T., Kirkevåg, A., Seland, Ø., et al. (2013). The Norwegian Earth system model, NorESM1-M—Part 1: Description and basic evaluation of the physical climate. *Geoscientific Model Development*, *6*(3), 687–720. https://doi.org/10.5194/gmd-6-687-2013

Bernardello, R., Marinov, I., Palter, J. B., Sarmiento, J. L., Galbraith, E. D., & Slater, R. D. (2014). Response of the ocean natural carbon storage to projected twenty-first-century climate change. *Journal of Climate*, *27*(5), 2033–2053. https://doi.org/10.1175/jcli-d-13-00343.1

Bopp, L., Resplandy, L., Orr, J. C., Doney, S. C., Dunne, J. P., Gehlen, M., et al. (2013). Multiple stressors of ocean ecosystems in the 21st century: Projections with CMIP5 models. *Biogeosciences*, *10*(10), 6225–6245. https://doi.org/10.5194/bg-10-6225-2013

Boucher, O., Halloran, P., Burke, E., Doutriaux-Boucher, M., Jones, C., Lowe, J., et al. (2012). Reversibility in an Earth System model in response to CO_2 concentration changes. *Environmental Research Letters*, *7*(2), 024013. https://doi.org/10.1088/1748-9326/7/2/024013

Box, J., Fettweis, X., Stroeve, J., Tedesco, M., Hall, D., & Steffen, K. (2012). Greenland ice sheet albedo feedback: Thermodynamics and atmospheric drivers. *The Cryosphere*, *6*(4), 821–839. https://doi.org/10.5194/tc-6-821-2012

Brewer, P. G., & Peltzer, E. T. (2016). Ocean chemistry, ocean warming, and emerging hypoxia: Commentary. *Journal of Geophysical Research: Oceans*, *121*(5), 3659–3667. https://doi.org/10.1002/2016jc011651

Brewer, P. G., & Peltzer, E. T. (2017). Depth perception: The need to report ocean biogeochemical rates as functions of temperature, not depth. *Philosophical Transactions of the Royal Society A: Mathematical, Physical & Engineering Sciences*, *375*(2102), 20160319. https://doi.org/10.1098/rsta.2016.0319

Brito-Morales, I., Schoeman, D. S., Molinos, J. G., Burrows, M. T., Klein, C. J., Arafeh-Dalmau, N., et al. (2020). Climate velocity reveals increasing exposure of deep-ocean biodiversity to future warming. *Nature Climate Change*, *10*(6), 576–581. https://doi.org/10.1038/s41558-020-0773-5

Buhl-Mortensen, L., Olafsdottir, S. H., Buhl-Mortensen, P., Burgos, J. M., & Ragnarsson, S. A. (2015). Distribution of nine cold-water coral species (Scleractinia and Gorgonacea) in the cold temperate North Atlantic: Effects of bathymetry and hydrography. *Hydrobiologia*, *759*(1), 39–61. https://doi.org/10.1007/s10750-014-2116-x

Caesar, L., Rahmstorf, S., & Feulner, G. (2020). On the relationship between Atlantic meridional overturning circulation slowdown and global surface warming. *Environmental Research Letters*, *15*(2), 024003. https://doi.org/10.1088/1748-9326/ab63e3

Cao, L., Zhang, H., Zheng, M., & Wang, S. (2014). Response of ocean acidification to a gradual increase and decrease of atmospheric CO 2. *Environmental Research Letters*, *9*(2), 024012. https://doi.org/10.1088/1748-9326/9/2/024012

Chen, X., & Tung, K.-K. (2018). Global surface warming enhanced by weak Atlantic overturning circulation. *Nature*, *559*(7714), 387. https://doi.org/10.1038/s41586-018-0320-y

Cheng, W., Chiang, J. C. H., & Zhang, D. (2013). Atlantic meridional overturning circulation (AMOC) in CMIP5 models: RCP and historical simulations. *Journal of Climate*, *26*(18), 7187–7197. https://doi.org/10.1175/jcli-d-12-00496.1

Coll, M., Steenbeek, J., Pennino, M. G., Buszowski, J., Kaschner, K., Lotze, H. K., et al. (2020). Advancing global ecological modeling capabilities to simulate future trajectories of change in marine ecosystems. *Frontiers in Marine Science*, *7*, 741. https://doi.org/10.3389/fmars.2020.567877

Costello, M. J., McCrea, M., Freiwald, A., Lundälv, T., Jonsson, L., Bett, B. J., et al. (2005). Role of cold-water Lophelia pertusa coral reefs as fish habitat in the NE Atlantic, In *Cold-water corals and ecosystems*, edited, pp. 771–805, Springer. https://doi.org/10.1007/3-540-27673-4_41

Courtney, T. A., Lebrato, M., Bates, N. R., Collins, A., De Putron, S. A., Garley, R., et al. (2017). Environmental controls on modern scleractinian coral and reef-scale calcification. *Science Advances*, *3*(11), e1701356. https://doi.org/10.1126/sciadv.1701356

Dagan, G., Stier, P., & Watson-Parris, D. (2020). Aerosol forcing masks and delays the formation of the north Atlantic warming hole by three decades. *Geophysical Research Letters*, *47*(22), e2020GL090778. https://doi.org/10.1029/2020GL090778

Danabasoglu, G., Lamarque, J. F., Bacmeister, J., Bailey, D., DuVivier, A., Edwards, J., et al. (2020). The community Earth system model version 2 (CESM2). *Journal of Advances in Modeling Earth Systems*, *12*(2), e2019MS001916. https://doi.org/10.1029/2019ms001916

Drijfhout, S., Oldenborgh, G. J. V., & Cimatoribus, A. (2012). Is a decline of AMOC causing the warming hole above the north Atlantic in observed and modeled warming patterns? *Journal of Climate*, *25*(24), 8373–8379. https://doi.org/10.1175/jcli-d-12-00490.1

Dunne, J., Horowitz, L., Adcroft, A., Ginoux, P., Held, I., John, J., et al. (2020). The GFDL Earth System Model version 4.1 (GFDL-ESM 4.1): Overall coupled model description and simulation characteristics. *Journal of Advances in Modeling Earth Systems*, *12*(11), e2019MS002015. https://doi.org/10.1029/2019ms002015

FAO. (2018). The state of world fisheries and aquaculture 2018-meeting the sustainable development goals, *edited*, FAO Rome.

Fransner, F., Fröb, F., Tjiputra, J., Goris, N., Lauvset, S. K., Skjelvan, I., et al. (2022). Acidification of the Nordic Seas. *Biogeosciences*, *19*(3), 979–1012. https://doi.org/10.5194/bg-19-979-2022

Friedlingstein, P., Andrew, R. M., Rogelj, J., Peters, G. P., Canadell, J. G., Knutti, R., et al. (2014). Persistent growth of CO_2 emissions and implications for reaching climate targets. *Nature Geoscience*, *7*(10), 709–715. https://doi.org/10.1038/ngeo2248

Garcia, H., & Gordon, L. I. (1992). Oxygen solubility in seawater: Better fitting equations. *Limnology & Oceanography*, *37*(6), 1307–1312. https://doi.org/10.4319/lo.1992.37.6.1307

Garcia, H., Locarnini, R., Boyer, T., Antonov, J., Zweng, M., Baranova, O., & Johnson, D. (2010). World Ocean Atlas 2009. In S.Levitus (Ed.), *Nutrients (Phosphate, Nitrate, Silicate). NOAA Atlas NESDIS, US Gov* (Vol. 4, p. 71. Printing Office, Wash.

Gasser, T., Guivarch, C., Tachiiri, K., Jones, C., & Ciais, P. (2015). Negative emissions physically needed to keep global warming below 2 C. *Nature Communications*, *6*(1), 1–7. https://doi.org/10.1038/ncomms8958

Gehlen, M., Séférian, R., Jones, D. O., Roy, T., Roth, R., Barry, J., et al. (2014). Projected pH reductions by 2100 might put deep North Atlantic biodiversity at risk. *Biogeosciences*, *11*(23), 6955–6967. https://doi.org/10.5194/bg-11-6955-2014

Goris, N., Tjiputra, J., Schwinger, J., & Heinze, C. (2015). Responses of carbon uptake and oceanic pCO_2 to climate change in the north Atlantic: A model study with the Bergen Earth system model. *Global Biogeochemical Cycles*, *29*(10), 1567–1583. https://doi.org/10.1002/2015gb005109

Guinotte, J. M., Orr, J., Cairns, S., Freiwald, A., Morgan, L., & George, R. (2006). Will human-induced changes in seawater chemistry alter the distribution of deep-sea scleractinian corals? *Frontiers in Ecology and the Environment*, *4*(3), 141–146. https://doi.org/10.1890/1540-9295(2006)004[0141:Whcisc]2.0.Co;2

Hameau, A., Mignot, J., & Joos, F. (2019). Assessment of time of emergence of anthropogenic deoxygenation and warming: Insights from a CESM simulation from 850 to 2100 CE. *Biogeosciences*, *16*, 1755–1780. https://doi.org/10.5194/bg-16-1755-2019

Hebbeln, D., Portilho-Ramos, R. d. C., Wienberg, C., & Titschack, J. (2019). The fate of cold-water corals in a changing world: A geological perspective. *Frontiers in Marine Science*, *6*(119), 1–8. https://doi.org/10.3389/fmars.2019.00119

Hennige, S. J., Wicks, L. C., Kamenos, N. A., Perna, G., Findlay, H. S., & Roberts, J. M. (2015). Hidden impacts of ocean acidification to live and dead coral framework, *Proceedings of the Royal Society B: Biological Sciences*, *282*(1813), 20150990. https://doi.org/10.1098/rspb.2015.0990

Henry, L.-A., Navas, J. M., Hennige, S. J., Wicks, L. C., Vad, J., & Roberts, J. M. (2013). Cold-water coral reef habitats benefit recreationally valuable sharks. *Biological Conservation*, *161*, 67–70. https://doi.org/10.1016/j.biocon.2013.03.002

Henson, S. A., Beaulieu, C., Ilyina, T., John, J. G., Long, M., Seferian, R., et al. (2017). Rapid emergence of climate change in environmental drivers of marine ecosystems. *Nature Communications*, *8*,14682. https://doi.org/10.1038/ncomms14682

Hidalgo, M., & Browman, H. I. (2019). *Developing the knowledge base needed to sustainably manage mesopelagic resources*. Oxford University Press

Hofmann, M., Mathesius, S., Kriegler, E., van Vuuren, D., & Schellnhuber, H. (2019). Strong time dependence of ocean acidification mitigation by atmospheric carbon dioxide removal. *Nature Communications*, *10*(1), 1–10. https://doi.org/10.1038/s41467-019-13586-4

IPCC. (2019). Summary for Policymakers. In H.-O. Pörtner, D. C. Roberts, V. Masson-Delmotte, P. Zhai, M. Tignor, E. Poloczanska, et al. (Eds.), *IPCC Special Report on the Ocean and Cryosphere in a Changing Climate* (pp. 3–35). Cambridge University Press. https://doi.org/10.1017/9781009157964.001

Irigoien, X., Klevjer, T. A., Røstad, A., Martinez, U., Boyra, G., Acuña, J., et al. (2014). Large mesopelagic fishes biomass and trophic efficiency in the open ocean. *Nature Communications*, *5*, 3271.

John, J. G., Stock, C. A., & Dunne, J. P. (2015). A more productive, but different, ocean after mitigation. *Geophysical Research Letters*, *42*(22), 9836–9845.

Jones, D. O., Yool, A., Wei, C. L., Henson, S. A., Ruhl, H. A., Watson, R. A., & Gehlen, M. (2014). Global reductions in seafloor biomass in response to climate change. *Global Change Biology*, *20*(6), 1861–1872

Katavouta, A., & Williams, R. G. (2021). Ocean carbon cycle feedbacks in CMIP6 models: Contributions from different basins. *Biogeosciences*, *18*(10), 3189–3218. https://doi.org/10.5194/bg-18-3189-2021

Keeling, C. D., Piper, S. C., Bacastow, R. B., Wahlen, M., Whorf, T. P., Heimann, M., & Meijer, H. A. (2005). Atmospheric CO_2 and $_{13}CO_2$ exchange with the terrestrial biosphere and oceans from 1978 to 2000: Observations and carbon cycle implications. In I. T.Baldwin (Ed.), et al. (Eds.), *A history of atmospheric CO2 and its effects on plants, animals, and ecosystems* (pp. 83–113). Springer New York. https://doi.org/10.1007/0-387-27048-5_5

Keil, P., Mauritsen, T., Jungclaus, J., Hedemann, C., Olonscheck, D., & Ghosh, R. (2020). Multiple drivers of the North Atlantic warming hole. *Nature Climate Change*, *10*(7), 667–671. https://doi.org/10.1038/s41558-020-0819-8

Keller, D. P., Lenton, A., Scott, V., Vaughan, N. E., Bauer, N., Ji, D., et al. (2018). The carbon dioxide removal model intercomparison project (CDRMIP): Rationale and experimental protocol for CMIP6. *Geoscientific Model Development*, *11*(3), 1133–1160.

Keller, F. J., & Raible, C. (2014). Time of emergence of trends in ocean biogeochemistry. *Biogeosciences*, *11*(13), 3647–3659.

Key, R. M., Kozyr, A., Sabine, C. L., Lee, K., Wanninkhof, R., Bullister, J. L., et al. (2004). A global ocean carbon climatology: Results from global data analysis project (GLODAP). *Global Biogeochemical Cycles*, *18*(4), G4301.

Kirkevåg, A., Iversen, T., Seland, Ø., Hoose, C., Kristjánsson, J., Struthers, H., et al. (2012). Aerosol-climate interactions in the Norwegian Earth system model–NorESM. *Geoscientific Model Development Discussions*, *5*(3), 2599–2685.

Krumhardt, K. M., Long, M. C., Lindsay, K., & Levy, M. N. (2020). Southern Ocean calcification controls the global distribution of alkalinity. *Global Biogeochemical Cycles*, *34*(12),e2020GB006727.

Kwiatkowski, L., Torres, O., Bopp, L., Aumont, O., Chamberlain, M., Christian, J. R., et al. (2020). Twenty-first century ocean warming, acidification, deoxygenation, and upper-ocean nutrient and primary production decline from CMIP6 model projections. *Biogeosciences*, *17*(13), 3439–3470.

Langehaug, H. R., Rhines, P. B., Eldevik, T., Mignot, J., & Lohmann, K. (2012). Water mass transformation and the North Atlantic Current in three multicentury climate model simulations. *Journal of Geophysical Research: Oceans*, *117*(C11), C11001.

Levin, L. A., & Le Bris, N. (2015). The deep ocean under climate change. *Science*, *350*(6262), 766–768. https://doi.org/10.1126/science.aad0126

Liu, M., & Tanhua, T. (2019). Distribution of water masses in the Atlantic ocean based on GLODAPv2. *Ocean Science Discussions*, 1–32.

Mahowald, N. M., Baker, A. R., Bergametti, G., Brooks, N., Duce, R. A., Jickells, T. D., et al. (2005). Atmospheric global dust cycle and iron inputs to the ocean. *Global Biogeochemical Cycles*, *19*(4), GB4025.

Maier-Reimer, E., Kriest, I., Segschneider, J., & Wetzel, P. (2005). *The Hamburg Ocean Carbon Cycle Model Hamocc5* (Vol. 1). technical description release 1.1.

McDougall, T. J., & Barker, P. M. (2011). Getting started with TEOS-10 and the Gibbs Seawater (GSW) oceanographic toolbox. *SCOR/IAPSO WG*, *127*, 1–28.

Meyer, J., & Riebesell, U. (2015). Reviews and syntheses: Responses of coccolithophores to ocean acidification: A meta-analysis. *Biogeosciences*, *12*(6), 1671–1682. https://doi.org/10.5194/bg-12-1671-2015

Oschlies, A., Brandt, P., Stramma, L., & Schmidtko, S. (2018). Drivers and mechanisms of ocean deoxygenation. *Nature Geoscience*, *11*(7), 467–473.

Puerta, P., Johnson, C., Carreiro-Silva, M., Henry, L.-A., Kenchington, E., Morato, T., et al. (2020). Influence of water masses on the biodiversity and biogeography of deep-sea benthic ecosystems in the north Atlantic. *Frontiers in Marine Science*, *7*, 239.

Ramirez-Llodra, E., Tyler, P. A., Baker, M. C., Bergstad, O. A., Clark, M. R., Escobar, E., et al. (2011). Man and the last great wilderness: Human impact on the deep sea. *PLoS One*, *6*(8), e22588.

Riebesell, U., Aberlehn-Malzahn, N., Achterberg, E. P., Algeuro-Muniz, M., Alvarez-Fernandez, S., Arestegui, J., et al. (2018). Toxic algal bloom induced by ocean acidification disrupts the pelagic food web. *Nature Climate Change*, *8*(12), 1082–1086. https://doi.org/10.1038/s41558-018-0344-1

Roquet, F., Madec, G., McDougall, T. J., & Barker, P. M. (2015). Accurate polynomial expressions for the density and specific volume of seawater using the TEOS-10 standard. *Ocean Modelling*, *90*, 29–43. https://doi.org/10.1016/j.ocemod.2015.04.002

Sarmiento, J. L., & Le Quere, C. (1996). Oceanic carbon dioxide uptake in a model of century-scale global warming. *Science*, *274*(5291), 1346–1350.

Schwinger, J., & Tjiputra, J. F. (2018). Ocean carbon cycle feedbacks under negative emissions. *Geophysical Research Letters*, *45*(10), 5062–5070.

Séférian, R., Nabat, P., Michou, M., Saint-Martin, D., Voldoire, A., Colin, J., et al. (2019). Evaluation of CNRM Earth system model, CNRM-ESM2-1: Role of Earth system processes in present-day and future climate. *Journal of Advances in Modeling Earth Systems*, *11*(12), 4182–4227.

Silvy, Y., Guilyardi, E., Sallée, J.-B., & Durack, P. J. (2020). Human-induced changes to the global ocean water masses and their time of emergence. *Nature Climate Change*, *10*(11), 1030–1036.

Smeed, D., McCarthy, G., Cunningham, S., Frajka-Williams, E., Rayner, D., Johns, W. E., et al. (2014). Observed decline of the Atlantic meridional overturning circulation 2004–2012. *Ocean Science*, *10*(1), 29–38.

Smith, P., Davis, S. J., Creutzig, F., Fuss, S., Minx, J., Gabrielle, B., et al. (2016). Biophysical and economic limits to negative CO 2 emissions. *Nature Climate Change*, *6*(1), 42–50.

Srokosz, M., Baringer, M., Bryden, H., Cunningham, S., Delworth, T., Lozier, S., et al. (2012). Past, present, and future changes in the Atlantic meridional overturning circulation. *Bulletin of the American Meteorological Society*, *93*(11), 1663–1676.

Steffen, W., Rockström, J., Richardson, K., Lenton, T. M., Folke, C., Liverman, D., et al. (2018). Trajectories of the Earth system in the Anthropocene. *Proceedings of the National Academy of Sciences*, *115*(33), 8252–8259.

Stendardo, I., & Gruber, N. (2012). Oxygen trends over five decades in the North Atlantic. *Journal of Geophysical Research: Oceans*, *117*(C11), C11004.

Swart, N. C., Cole, J. N., Kharin, V. V., Lazare, M., Scinocca, J. F., Gillett, N. P., et al. (2019). The Canadian Earth system model version 5 (CanESM5. 0.3). *Geoscientific Model Development*, *12*(11), 4823–4873.

Tjiputra, J. F., Assmann, K., Bentsen, M., Bethke, I., Otterå, O., Sturm, C., & Heinze, C. (2010). Bergen Earth system model (BCM-C): Model description and regional climate-carbon cycle feedbacks assessment. *Geoscientific Model Development*, *3*(1), 123–141.

Tjiputra, J. F., Assmann, K., & Heinze, C. (2010). Anthropogenic carbon dynamics in the changing ocean. *Ocean Science*, *6*(3), 605.

Tjiputra, J. F., Goris, N., Lauvset, S. K., Heinze, C., Olsen, A., Schwinger, J., & Steinfeldt, R. (2018). Mechanisms and early detections of multidecadal oxygen changes in the interior subpolar North Atlantic. *Geophysical Research Letters*, *45*(9), 4218–4229. https://doi.org/10.1029/2018gl077096

Tjiputra, J. F., Roelandt, C., Bentsen, M., Lawrence, D. M., Lorentzen, T., Schwinger, J., et al. (2013). Evaluation of the carbon cycle components in the Norwegian Earth system model (NorESM). *Geoscientific Model Development*, *6*(2), 301–325. https://doi.org/10.5194/gmd-6-301-2013

Tjiputra, J. F., Schwinger, J., Bentsen, M., Morree, A. L., Gao, S., Bethke, I., et al. (2020). Ocean biogeochemistry in the Norwegian Earth system model version 2 (NorESM2). *Geoscientific Model Development*, *13*(5), 2393–2431. https://doi.org/10.5194/gmd-13-2393-2020

Tokarska, K. B., & Zickfeld, K. (2015). The effectiveness of net negative carbon dioxide emissions in reversing anthropogenic climate change. *Environmental Research Letters*, *10*(9), 094013.

Trisos, C. H., Merow, C., & Pigot, A. L. (2020). The projected timing of abrupt ecological disruption from climate change. *Nature*, *580*(7804), 496–501.

Völker, C., Wallace, D. W., & Wolf-Gladrow, D. A. (2002). On the role of heat fluxes in the uptake of anthropogenic carbon in the North Atlantic. *Global Biogeochemical Cycles*, *16*(4), 8581–8589.

Wassmann, P., Duarte, C. M., Agusti, S., & Sejr, M. K. (2011). Footprints of climate change in the Arctic marine ecosystem. *Global Change Biology*, *17*(2), 1235–1249.

Webster, N. S., Negri, A. P., Botté, E. S., Laffy, P. W., Flores, F., Noonan, S., et al. (2016). Host-associated coral reef microbes respond to the cumulative pressures of ocean warming and ocean acidification. *Scientific Reports*, *6*,19324. https://doi.org/10.1038/srep19324

Weijer, W., Cheng, W., Garuba, O. A., Hu, A., & Nadiga, B. T. (2020). CMIP6 models predict significant 21st century decline of the Atlantic meridional overturning circulation. *Geophysical Research Letters*, *47*(12), e2019GL086075. https://doi.org/10.1029/2019GL086075

Whitt, D. B., & Jansen, M. F. (2020). Slower nutrient stream suppresses Subarctic Atlantic Ocean biological productivity in global warming. *Proceedings of the National Academy of Sciences*, *117*(27), 15504. https://doi.org/10.1073/pnas.2000851117

Winton, M., Griffies, S. M., Samuels, B. L., Sarmiento, J. L., & Frölicher, T. L. (2013). Connecting changing ocean circulation with changing climate. *Journal of Climate*, *26*(7), 2268–2278. https://doi.org/10.1175/jcli-d-12-00296.1

Zickfeld, K., Eby, M., & Weaver, A. J. (2008). Carbon-cycle feedbacks of changes in the Atlantic meridional overturning circulation under future atmospheric CO_2. *Global Biogeochemical Cycles*, *22*(3), GB3024.